Autonomous Robots (2020) 44:25–42
https://doi.org/10.1007/s10514-019-09850-7

Statistics of the distance traveled until successful connectivity for unmanned vehicles

Arjun Muralidharan[1] · **Yasamin Mostofi**[1]

Received: 2 August 2018 / Accepted: 6 April 2019 / Published online: 22 April 2019

Abstract
In this paper, we consider a scenario where a robot needs to establish connectivity with a remote operator or another robot, as it moves along a path. We are interested in answering the following question: what is the distance traveled by the robot along the path before it finds a connected spot? More specifically, we are interested in characterizing the statistics of the distance traveled along the path before it gets connected, in realistic channel environments experiencing path loss, shadowing and multipath effects. We develop an exact mathematical analysis of these statistics for straight-line paths and also mathematically characterize a more general space of loop-free paths (beyond straight paths) for which the analysis holds, based on the properties of the path such as its curvature. Finally, we confirm our theoretical analysis using extensive numerical results with real channel parameters from downtown San Francisco.

Keywords First passage distance · Connectivity · Mobile robots · Gauss–Markov process · Realistic communication

1 Introduction

There has been considerable research on a team of unmanned vehicles carrying out a wide range of tasks such as search and rescue, surveillance, agriculture, and environment monitoring (Tokekar et al. 2016; Yan and Mostofi 2014). Communication between such a team of robots and a remote operator or within the robotic network itself, is often crucial for the successful completion of these tasks. For instance, consider a scenario where a robot has collected information about its environment and needs to transmit this information to a remote operator or another robot. In order to do so, it first needs to establish a connection with the remote operator or the other robot. The robot may not be able to do so at its current location and may need to move to establish a connection, exploiting the spatial variations of the channel quality. This paper then answers the following question: what are the statistics of the distance traveled along a given path until connectivity?

There has been considerable recent interest in the area of connectivity in robotic systems. For instance, in Zavlanos et al. (2011), the connectivity of a network is maximized using a graph-theoretic analysis while in Yan and Mostofi (2012), connectivity is optimized using a more realistic channel model. In Abbasi et al. (2009), a minimal set of nodes are identified for repositioning, in order to reestablish connectivity in a wireless mobile sensor network. There has also been work on path planning to enable connectivity (Caccamo et al. 2017; Chatzipanagiotis and Zavlanos 2016; Muralidharan and Mostofi 2017a, c; Yan and Mostofi 2012; Zeng and Zhang 2017) as well as on communication-aware sensing (Yan and Mostofi 2014). In Muralidharan and Mostofi (2017c), path planning for an initially unconnected robot is carried out such that it gets connected to a remote operator, and in Caccamo et al. (2017), comm-aware trajectory planning with a connectivity repair heuristic is carried out. In Zeng and Zhang (2017), an energy efficient trajectory is designed for a UAV communicating with a remote station.

This work is supported in part by NSF CCSS award 1611254 and NSF RI award 1619376.

This is one of the several papers published in *Autonomous Robots* comprising Special Issue on Robot Communication Challenges: Real-World Problems, Systems, and Methods.

✉ Arjun Muralidharan
arjunm@ece.ucsb.edu

Yasamin Mostofi
ymostofi@ece.ucsb.edu

[1] Department of Electrical and Computer Engineering, University of California Santa Barbara, Santa Barbara, CA 93106, USA

However, a mathematical characterization of the statistics of the distance traveled until connectivity is lacking in the literature, which is the main motivation for this paper. We refer to this problem as *the first passage distance (FPD) problem*, analogous to the concept of first passage time (Siegert 1951). We next summarize the contributions of the paper.

Statement of contributions We mathematically characterize the probability density function (PDF) of the FPD as a function of the underlying channel parameters of the environment, such as shadowing, path loss, and multipath fading parameters. We do so for two cases: (1) when ignoring the multipath component (which could be of interest when the robot looks for an area of good connectivity as opposed to a single spot, or when multipath is negligible), and (2) when considering the multipath component. In both cases, we first develop an exact characterization of the statistics of the FPD for the setting with straight paths. We utilize tools from the stochastic equation literature to characterize the FPD while ignoring the multipath component, and develop a recursive characterization for the case when we include multipath. We then mathematically characterize a more general space of paths for which the analysis holds, based on properties of the path such as its curvature.

Note that the PDF of the FPD can be directly computed via a high dimensional integration, as we will discuss in Sect. 4.1. However, this direct computation is infeasible for moderate distances. Our proposed theoretical framework is not only computationally efficient but also brings a foundational analytical understanding to the FPD and can significantly affect networked robotic operation design. The analysis can further help with the operation on the field and the design of robotic paths. For instance, consider the scenario of a robot on a field mission that is tasked with sensing an area and communicating the collected data to a remote node or a human operator. The robot may then need to find a connected spot after it has collected its data. By using our proposed framework, the robot can estimate the statistics of the distance traveled until it establishes communication. Furthermore, the derivations can be used to explicitly co-optimize and design robotic sensing and path planning as part of future work. We finally emphasize that the derivations of the paper are applicable to both cases of trying to establish communication with remote operators as well as trying to establish communication with another robot.

A small part of this paper has appeared in Muralidharan and Mostofi (2017b), in which we characterized the statistics of the distance traveled until connectivity, only for straight-line paths. In contrast, in this paper, we have extensively extended this analysis and developed new mathematical tools to tackle a more general space of paths. Moreover, for the case where we consider multipath in Sect. 4, we have proposed a new methodology to compute the statistics, which is significantly more efficient. Finally, on the numerical results side, we have extensive validation of our theoretical analysis, with real channel measurements.

The paper is organized as follows. In Sect. 2, we formally introduce the problem and briefly summarize the channel's underlying dynamics. In Sect. 3, we characterize the statistics of the distance traveled until connectivity while ignoring the multipath component. In Sect. 4, we characterize the statistics of the FPD while including the effect of multipath in the analysis. Finally, in Sect. 5, we validate our mathematical characterizations through extensive simulation with real channel parameters from downtown San Francisco.

2 Problem setup

Consider a robot traveling along a given trajectory that needs to get connected to either a remote operator or another robot, as shown in Fig. 1a. In order for the robot to successfully connect with the remote operator, the receptions need to satisfy a Quality of Service (QoS) requirement such as a target Bit Error Rate, which in turn results in a minimum required received Signal to Noise Ratio, or equivalently a minimum required channel power, given a fixed transmission power. We denote this minimum required received channel power as γ_{th} in this paper. This paper then asks the following question: *What is the distance traveled by the robot along the path before it gets connected to the remote operator?* More specifically, we are interested in mathematically characterizing the probability density function (PDF) of this distance, for a given path, as a function of the underlying channel parameters, such as path loss, shadowing and multipath fading parameters, as well as the parameters of the path, such as its curvature. Throughout the analysis, we assume that the robot can localize itself with respect to the remote operator (or the other robot) that it is trying to establish a connection with.

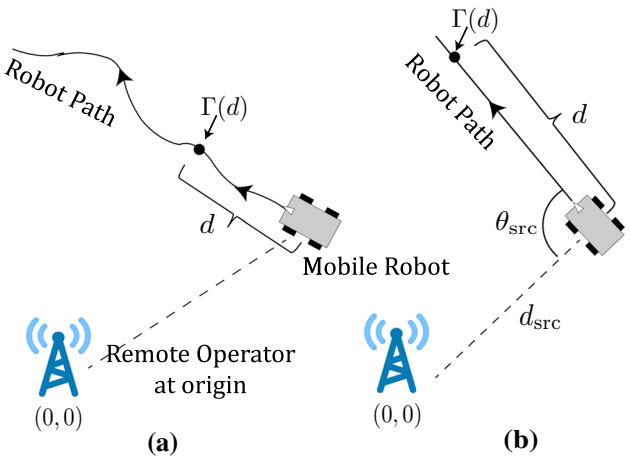

Fig. 1 An example of the considered scenario for **a** a general path and **b** a straight path

2.1 Channel model

In the communication literature, channel power is well modeled as a multi-scale random process with three major dynamics: path loss, shadowing and multipath fading (Rappaport 1996). Let $\Gamma_{\mathrm{O}}(q)$ represent the received channel power (in the dB domain) at location $q \in \mathbb{R}^2$ with the remote operator located at the origin. $\Gamma_{\mathrm{O}}(q)$ can then be expressed as $\Gamma_{\mathrm{O}}(q) = \gamma_{\mathrm{O,PL}}(q)+\Gamma_{\mathrm{O,SH}}(q)+\Gamma_{\mathrm{O,MP}}(q)$ where $\gamma_{\mathrm{O,PL}}(q) = K_{\mathrm{dB}} - 10n_{\mathrm{PL}}\log_{10}\|q\|$ is the distance-dependent path loss with n_{PL} representing the path loss exponent, and $\Gamma_{\mathrm{O,SH}}$ and $\Gamma_{\mathrm{O,MP}}$ are random variables denoting the impact of shadowing and multipath respectively (in dB). The multipath component or small-scale fading represents fluctuations in the channel power in the order of a wavelength, while the shadowing component or large-scale fading represents fluctuations of the channel power after the signal is locally averaged over multipath, thus reflecting the impact of larger objects such as blocking buildings. $\Gamma_{\mathrm{O,SH}}(q)$ is best modeled as a Gaussian random process with an exponential spatial correlation, i.e., $\mathbb{E}\left\{\Gamma_{\mathrm{O,SH}}(q_1)\Gamma_{\mathrm{O,SH}}(q_2)\right\} = \sigma^2_{\mathrm{SH}}e^{-\|q_1-q_2\|/\beta_{\mathrm{SH}}}$ where σ^2_{SH} is the shadowing power and β_{SH} is the decorrelation distance (Rappaport 1996). As for multipath, a number of distributions such as Nakagami, Rician and lognormal have been found to be a good fit (in the linear domain) (Hashemi 1994; Rappaport 1996).

Consider the case where the robot is traveling along a path. Let d be the distance traveled by the robot along this path. We let $\Gamma(d)$ represent the channel power when the robot has traveled distance d along the path, as marked in Fig. 1a. We thus have $\Gamma(d) = \gamma_{\mathrm{PL}}(d) + \Gamma_{\mathrm{SH}}(d) + \Gamma_{\mathrm{MP}}(d)$.

3 Characterizing the FPD without considering multipath

We start our analysis by ignoring the multipath and only considering the shadowing and path loss components of the channel, i.e., we want $\Gamma(d) = \gamma_{\mathrm{PL}}(d) + \Gamma_{\mathrm{SH}}(d)$ to be above γ_{th}. This assumption allows us to better analyze and understand the FPD, and paves the way towards our most general characterization of the next section, which includes multipath as well. Moreover, the analysis also has practical values of its own, and would be relevant to the case where the robot is interested in finding a general area of good connectivity as opposed to a single good spot. In this section, we will characterize the statistics of the distance traveled until connectivity for this scenario. We begin by analyzing straight paths in Sect. 3.1, where we utilize the stochastic differential equation literature (Gardiner 2009) in our characterization. We then extend our analysis to a more general space of paths in Sect. 3.2.

3.1 Straight paths: stochastic differential equation analysis

In this section, we characterize the PDF of the distance traveled until connectivity for straight-line paths. Consider a robot situated at a distance d_{src} from a remote operator or from another robot to which it needs to be connected, and moving in the direction specified by the angle θ_{src}, as shown in Fig. 1b. The angle θ_{src} is measured clockwise with respect to the line segment connecting the remote operator and the robot, as can be seen in Fig. 1b, and denotes the direction of travel chosen by the robot.

$\Gamma(d)$ represents the channel power when the robot is at distance d along direction θ_{src}, as marked in Fig. 1b. We thus have $\Gamma(d) = \gamma_{\mathrm{PL}}(d) + \Gamma_{\mathrm{SH}}(d)$, where

$$\gamma_{\mathrm{PL}}(d) = K_{\mathrm{dB}} - 5n_{\mathrm{PL}}\log_{10}(d^2_{\mathrm{src}} + d^2 - 2d_{\mathrm{src}}d\cos\theta_{\mathrm{src}}), \tag{1}$$

which follows from the geometry of the setting. Moreover, $\Gamma_{\mathrm{SH}}(d)$ is a zero mean Gaussian process with the spatial correlation of $\mathbb{E}\{\Gamma_{\mathrm{SH}}(l)\Gamma_{\mathrm{SH}}(d)\} = \sigma^2_{\mathrm{SH}}e^{-(d-l)/\beta_{\mathrm{SH}}}$, with $d \geq l$. Note that $\Gamma(d)$ is also a function of d_{src} and θ_{src}. We drop $\Gamma(d)$'s dependency on them in the notation as the analysis of the paper is carried out for a fixed d_{src} and θ_{src}.

As we shall see, $\Gamma_{\mathrm{SH}}(d)$ becomes an Ornstein–Uhlenbeck process, one of the most studied types of Gauss–Markov processes (Gardiner 2009; Leblanc and Scaillet 1998; Ricciardi and Sacerdote 1979; Ricciardi and Sato 1988). Ornstein–Uhlenbeck process appears in many practical scenarios, such as Brownian motion, financial stock markets, or neuronal firing (Ricciardi and Sacerdote 1979; Leblanc and Scaillet 1998), and thus has been heavily studied in the literature. In this paper, we shall utilize this rich literature (Gardiner 2009; Di Nardo et al. 2001) to mathematically characterize the FPD to connectivity for a mobile robot.

We begin by summarizing the definitions of a Gaussian process and a Markov process.

Definition 1 *(Gaussian Process)* (Dudley 2002) A stochastic process $\{X(t) : t \in T\}$, where T is an index set, is a Gaussian process, if any finite number of samples have a joint Gaussian distribution, i.e., $(X(t_1), X(t_2), \ldots, X(t_k))$ is a Gaussian random vector for all $t_1, \ldots, t_k \in T$ and for all k.

A Gaussian process is completely specified by its mean function $\mu(t) = \mathbb{E}[X(t)]$ and its covariance function $C(s,t) = \mathbb{E}\{[X(s) - \mu(s)][X(t) - \mu(t)]\}$. We use the notation $X \sim \mathcal{GP}(\mu, C)$ to denote the underlying process.

Definition 2 *(Markov Process)* (Papoulis and Pillai 2002) A process $X(t)$ is Markov if

$$\Pr\left(X(t_n) \leq x_n | X(t_{n-1}), \ldots, X(t_1)\right) = \Pr\left(X(t_n) \leq x_n | X(t_{n-1})\right),$$

for all n and for all $t_n \geq t_{n-1} \geq \cdots \geq t_1$, where $\Pr(.)$ denotes the probability of the argument.

Definition 3 *(Gauss–Markov Process)* (Mehr and McFadden 1965) A stochastic process is Gauss–Markov if it satisfies the requirements of both a Gaussian process and a Markov process.

We next state a lemma that shows when a Gaussian process is also Markov, which we shall utilize to prove that the channel shadowing power $\Gamma_{\text{SH}}(d)$ is Gauss–Markov.

Lemma 1 *A Gaussian process $X \sim \mathcal{GP}(\mu, C)$ is Markov if and only if $C(s,u) = C(s,t)C(t,u)/C(t,t)$, for all $u \geq t \geq s$.*

Proof See Doob (1949) for the proof. □

Corollary 1 *The channel shadowing power $\Gamma_{SH}(d)$ and the channel power $\Gamma(d)$ are Gauss–Markov processes.*

Proof $\Gamma_{\text{SH}} \sim \mathcal{GP}(0, C_{\Gamma_{\text{SH}}})$ is a Gaussian process with zero mean and covariance $C_{\Gamma_{\text{SH}}}(s,u) = \sigma^2_{\text{SH}} e^{-(u-s)/\beta_{\text{SH}}}$. This covariance function satisfies $C_{\Gamma_{\text{SH}}}(s,t)C_{\Gamma_{\text{SH}}}(t,u)/C_{\Gamma_{\text{SH}}}(t,t) = \sigma^2_{\text{SH}} e^{-(u-t)-(t-s)/\beta_{\text{SH}}} = C_{\Gamma_{\text{SH}}}(s,u)$, for $u \geq t \geq s$, which concludes the proof for $\Gamma_{\text{SH}}(d)$ using Lemma 1. The channel power $\Gamma(d)$ is the sum of $\Gamma_{\text{SH}}(d)$ and a mean function (path loss function $\gamma_{\text{PL}}(d)$). Thus, the channel power is also a Gauss–Markov process with distribution $\Gamma \sim \mathcal{GP}(\gamma_{\text{PL}}, C_{\Gamma_{\text{SH}}})$. □

Remark 1 (see Gardiner 2009) The Ornstein–Uhlenbeck process $O \sim \mathcal{GP}(0, C_O)$ is a Gauss–Markov process with the covariance function $C_O(s,u) = \sigma^2 e^{-(u-s)/\beta}$, where $\sigma \geq 0$ and $\beta \geq 0$ are constants. Thus, we can see that $\Gamma_{\text{SH}}(d)$ is an Ornstein–Uhlenbeck process.

In order to gain more insight into the stochastic process $\Gamma(d)$, we next discuss the transition PDF $f(\gamma, d|\eta, l) = \frac{\partial}{\partial \gamma} \Pr\left(\Gamma(d) < \gamma | \Gamma(l) = \eta\right)$, where $d \geq l$, as well as the stochastic differential equation governing $\Gamma(d)$, both of which we shall subsequently use in our characterization of the PDF of the FPD.

3.1.1 The underlying stochastic differential equation

The transition PDF $f(\gamma, d|\eta, l)$ characterizes the distribution of $\Gamma(d)$ given $\Gamma(l) = \eta$. This is a normal density characterized by a mean and variance of (see 10.5 of Kay 1993)

$$\begin{aligned} \mathbb{E}\left[\Gamma(d)|\Gamma(l) = \eta\right] &= \gamma_{\text{PL}}(d) + e^{-(d-l)/\beta_{\text{SH}}}(\eta - \gamma_{\text{PL}}(l)) \\ \text{Var}\left[\Gamma(d)|\Gamma(l) = \eta\right] &= \sigma^2_{\text{SH}}(1 - e^{-2(d-l)/\beta_{\text{SH}}}). \end{aligned} \tag{2}$$

The transition PDF explicitly shows the spatial dependence of the channel power $\Gamma(d)$. As stated in Di Nardo et al. (2001), $f(\gamma, d|\eta, l)$ satisfies the partial differential equation known as the forward Fokker–Planck equation[1]:

$$\frac{\partial}{\partial d} f(\gamma, d|\eta, l) = -\frac{\partial}{\partial \gamma}\left[A(\gamma, d) f(\gamma, d|\eta, l)\right] + \frac{1}{2}\frac{\partial^2}{\partial \gamma^2}\left[B f(\gamma, d|\eta, l)\right], \tag{3}$$

with the associated initial condition of $f(\gamma, l|\eta, l) = \delta(\gamma - \eta)$, where $A(\gamma, d) = \gamma'_{\text{PL}}(d) - (\gamma - \gamma_{\text{PL}}(d))/\beta_{\text{SH}}$, $B = (2\sigma^2_{\text{SH}})/\beta_{\text{SH}}$ and $\gamma_{\text{PL}}(d)$ is as stated in (1), with its derivative:

$$\gamma'_{\text{PL}}(d) = -10 n_{\text{PL}} \log_{10}(e) \frac{d - d_{\text{src}} \cos\theta_{\text{src}}}{d^2_{\text{src}} + d^2 - 2 d_{\text{src}} d \cos\theta_{\text{src}}}.$$

The Fokker–Planck equation shows the evolution of the probability density $f(\gamma, d|\eta, l)$ with the traveled distance d given $\Gamma(l) = \eta$.

Moreover, as shown in Gardiner (2009), the channel power $\Gamma(d)$ can be represented as a stochastic differential equation[2]:

$$\text{d}\Gamma(d) = A(\Gamma, d)\text{d}d + \sqrt{B}\text{d}W(d), \tag{4}$$

where $W(d)$ is the Wiener process and $A(\gamma, d)$ and B are as defined before. The Wiener process is a continuous time stochastic process with independent Gaussian increments, i.e., for $d > l$, the increment $W(d) - W(l) \sim \mathcal{N}(0, d - l)$ is independent of past values $W(b)$, $b \leq l$.

Remark 2 In (3) and (4), $A(\gamma, d)$ and B are known as the drift and the diffusion components respectively. The drift $A(\gamma, d) = \gamma'_{\text{PL}}(d) - (\gamma - \gamma_{\text{PL}}(d))/\beta_{\text{SH}}$ is a pull towards the mean, and the diffusion component $B = (2\sigma^2_{\text{SH}})/\beta_{\text{SH}}$ is a function of the shadowing variance and the decorrelation distance. Then, in an increment Δd, we can think of the channel power spatially evolving with a deterministic rate $A(\gamma, d)$, in addition to a random Gaussian term with the variance $B\Delta d$.

Next, we utilize our established lemmas to derive the PDF of the FPD.

3.1.2 First passage distance

Consider the random variable $\mathcal{D}_{\gamma_0} = \inf_{d \geq 0}\{d : \Gamma(d) \geq \gamma_{\text{th}} | \Gamma(0) = \gamma_0 < \gamma_{\text{th}}\}$. This denotes the FPD of the process

[1] The Fokker–Planck equation of Di Nardo et al. (2001) is stated for a general Gauss–Markov process. Here we adapted it for our specific Gauss–Markov process $\Gamma(d)$.

[2] Gardiner (2009) provides the stochastic differential equation for the Ornstein–Uhlenbeck process, from which we can easily obtain (4).

$\Gamma(d)$ to the connectivity threshold γ_{th}, with the initial value $\Gamma(0) = \gamma_0 < \gamma_{\text{th}}$. Further, let $g[d|\gamma_0] = \frac{\partial}{\partial d}\Pr\left(\mathcal{D}_{\gamma_0} < d\right)$ represent the PDF of the FPD. In the following theorem, we characterize this PDF.

Theorem 1 *The PDF of FPD $g[d|\gamma_0]$ satisfies the following non-singular second-kind Volterra integral equation:*

$$g[d|\gamma_0] = -2\Psi[d|\gamma_0, 0] + 2\int_0^d g[l|\gamma_0]\Psi[d|\gamma_{th}, l]\mathrm{d}l, \quad (5)$$

where $\gamma_0 < \gamma_{th}$ and

$$\Psi[d|\eta, l] = \left\{ -\frac{1}{2}\frac{\mathrm{d}\gamma_{PL}(d)}{\mathrm{d}d} - \frac{\gamma_{th} - \gamma_{PL}(d)}{2\beta_{SH}}\frac{1 + e^{-2(d-l)/\beta_{SH}}}{1 - e^{-2(d-l)/\beta_{SH}}} + \frac{\eta - \gamma_{PL}(l)}{\beta_{SH}}\frac{e^{-(d-l)/\beta_{SH}}}{1 - e^{-2(d-l)/\beta_{SH}}} \right\} f(\gamma_{th}, d|\eta, l). \quad (6)$$

Proof The proof is based on the fact that $\Gamma(d)$ is a Gauss–Markov process and utilizes the Fokker–Planck equation (3). The details are then adapted from Theorem 3.1 of Di Nardo et al. (2001) to our particular Gauss–Markov process. □

$\mathcal{D}_{\gamma_0}$ represents the FPD for a given initial value of $\Gamma(0) = \gamma_0$. In many scenarios, we are instead interested in characterizing the FPD for the initial state $\Gamma(0)$ being a random variable bounded from above by γ_{th}, i.e., we are interested in characterizing the FPD when the starting position is not connected. This is known as the upcrossing FPD in the general first passage literature (Di Nardo et al. 2001). We next extend our analysis to derive the PDF of the upcrossing FPD. Let the random variable $\mathcal{D}_{\Gamma_0}^{(\epsilon)} = \inf_{d\geq 0}\{d : \Gamma(d) \geq \gamma_{\text{th}}|\Gamma(0) < \gamma_{\text{th}} - \epsilon\}$ denote the ϵ-upcrossing FPD of $\Gamma(d)$ to the boundary γ_{th} given that the initial state satisfies $\Gamma(0) < \gamma_{\text{th}} - \epsilon$, where $\epsilon > 0$ is a fixed real number. The ϵ-upcrossing FPD, $\mathcal{D}_{\Gamma_0}^{(\epsilon)}$, can be characterized as follows:

$$\Pr\left(\mathcal{D}_{\Gamma_0}^{(\epsilon)} < d\right) = \int_{-\infty}^{\gamma_{\text{th}}-\epsilon} \Pr\left(\mathcal{D}_{\gamma_0} < d\right)\zeta_\epsilon(\gamma_0)\mathrm{d}\gamma_0,$$

where $\mathcal{D}_{\gamma_0}$ is the FPD given the initial value $\Gamma(0) = \gamma_0 < \gamma_{\text{th}}$, as defined earlier, and

$$\zeta_\epsilon(\gamma_0) = \begin{cases} \frac{f(\gamma_0,0)}{\Pr(\Gamma(0)<\gamma_{\text{th}}-\epsilon)}, & \gamma_0 < \gamma_{\text{th}} - \epsilon \\ 0, & \gamma_0 \geq \gamma_{\text{th}} - \epsilon \end{cases},$$

is the PDF of $\Gamma(0)|\Gamma(0) < \gamma_{\text{th}} - \epsilon$ with $f(\gamma, d)$ denoting the PDF of $\Gamma(d)$. Moreover, the ϵ-upcrossing FPD density $g_u^{(\epsilon)}[d] = \frac{\partial}{\partial d}\mathrm{P}(\mathcal{D}_{\Gamma_0}^{(\epsilon)} < d)$ is similarly related to the FPD density $g[d|\gamma_0]$ as follows: $g_u^{(\epsilon)}[d] = \int_{-\infty}^{\gamma_{\text{th}}-\epsilon} g[d|\gamma_0]\zeta_\epsilon(\gamma_0)\mathrm{d}\gamma_0$.

Remark 3 Note that we have required $\epsilon > 0$. This is due to the fact that the mathematical tools we shall utilize are not well-defined for $\gamma_0 = \gamma_{\text{th}}$, i.e., ϵ-upcrossing FPD is not mathematically well defined for $\epsilon = 0$. However, ϵ can be chosen arbitrarily small.

In the following theorem, we derive an expression for $g_u^{(\epsilon)}[d]$, the PDF of the ϵ-upcrossing FPD.

Theorem 2 *The PDF of the ϵ-upcrossing FPD, $g_u^{(\epsilon)}[d]$, satisfies the following non-singular second-kind Volterra integral equation:*

$$g_u^{(\epsilon)}[d] = -2\Psi_u^{(\epsilon)}[d] + 2\int_0^d g_u^{(\epsilon)}[l]\Psi[d|\gamma_{th}, l]\mathrm{d}l, \quad (7)$$

where $\Psi[d|\eta, l]$ is as defined in (6),

$$\Psi_u^{(\epsilon)}[d] = \frac{1}{2\Pr(\Gamma(0) < \gamma_{th} - \epsilon)}\left\{ \frac{-2\sigma_{SH}^2}{\beta_{SH}} e^{-d/\beta_{SH}} f(\gamma_{th} - \epsilon, 0) \times f[\gamma_{th}, d|\gamma_{th} - \epsilon, 0] + \frac{1}{2}f(\gamma_{th}, d)(1 + \mathrm{Erf}[\Upsilon_\epsilon(d)]) \times \left(-\frac{\mathrm{d}\gamma_{PL}(d)}{\mathrm{d}d} - \frac{1}{\beta_{SH}}\left[\gamma_{th} - \gamma_{PL}(d)\right]\right)\right\},$$

with $\mathrm{Erf}(z) = \frac{2}{\sqrt{\pi}}\int_0^z e^{-t^2}\mathrm{d}t$ *representing the error function, and*

$$\Upsilon_\epsilon(d) = \frac{\gamma_{th} - \epsilon - \gamma_{PL}(0) - e^{-d/\beta_{SH}}\left(\gamma_{th} - \gamma_{PL}(d)\right)}{\sqrt{2\sigma_{SH}^2\left(1 - e^{-2d/\beta_{SH}}\right)}}.$$

Proof The proof is obtained by adapting Theorem 5.3 of Di Nardo et al. (2001) to our particular Gauss–Markov process form. □

In terms of implementation, the functions $\Psi[d|\eta, l]$ and $\Psi_u^\epsilon[d]$ in Theorems 1 and 2 can be easily computed. The PDF of the FPD ($g[d|\gamma_0]$) and the PDF of the ϵ-upcrossing FPD ($g_u^{(\epsilon)}[d]$) can then be computed from the integral equations (5) and (7) respectively. In particular, Simpson rule provides the basis for an efficient iterative algorithm for evaluating these integrals (See Section 4 of Di Nardo et al. 2001).

Remark 4 (Computational complexity) The direct computation of $g_u^{(\epsilon)}[d]$ involves a high dimension integration, as we will discuss in Sect. 4.1. For a discretized path of N steps, this direct computation would have a computational cost exponential in N, i.e. $O(NM^N)$ for some constant M. In contrast, the computation cost of $g_u^{(\epsilon)}[d]$ using Theorem 2 is $O(N^2)$. Moreover, Theorem 2 is also an elegant characterization of the ϵ-upcrossing FPD that can be utilized for analysis and design of robotic operations.

3.2 Approximately-Markovian paths

In this part, we summarize how the results of this section can be utilized to obtain the statistics of the FPD for a more general space of non-straight paths. As we saw in Sect. 3.1, the channel shadowing component along a straight line is a Gauss–Markov process. This allowed us to characterize the statistics of the distance to connectivity for a mobile robot traveling along a straight path. A general non-straight path is not Markovian since the covariance function $C_{\Gamma_{\text{SH}}}(s,u)$ does not satisfy Lemma 1. In this section, we characterize the space of paths for which the channel shadowing power along the path is approximately a Gauss–Markov process. This allows us to immediately apply the stochastic differential equation analysis of Sect. 3.1 to characterize the statistics of the distance until connectivity for these paths.

Consider the scenario in Fig. 2 (top), where we have discretized the path, with $\Gamma_{\text{SH},-0}$ denoting the shadowing power at the current location and $\Gamma_{\text{SH},-1}, \Gamma_{\text{SH},-2}, \ldots$ indicating the channel shadowing power at previously-visited points.[3] In Sect. 3.2, we saw that a Gauss–Markov process satisfies the Fokker–Planck equation of (3), which provides us with the result of Theorem 2. The Fokker–Planck equation in turn requires the property that $p(\gamma_{\text{SH},-0}|\gamma_{\text{SH},-1}, \gamma_{\text{SH},-2}, \ldots) = p(\gamma_{\text{SH},-0}|\gamma_{\text{SH},-1})$ for its derivation [through the Chapman–Kolmogorov equation (Gardiner 2009)]. Thus, we say a path is approximately-Markovian, if at every point on the path, we have that $p(\gamma_{\text{SH},-0}|\gamma_{\text{SH},-1}, \gamma_{\text{SH},-2}, \ldots)$ is close to $p(\gamma_{\text{SH},-0}|\gamma_{\text{SH},-1})$. We will characterize this closeness precisely in Sect. 3.2.2 using the Kullback–Leibler (KL) divergence metric.

Our key insight is that the approximate Markovian nature is related to the curvature of a path, which is a measure of how much the path curves, i.e., how much it deviates from a straight line. For instance, a straight line has a curvature of 0. Thus, we would expect that paths with small enough curvature would result in approximately-Markovian processes. We will precisely characterize what we mean by this in Sect. 3.2.4.

We first describe an outline of our approach for characterizing the space of approximately-Markovian paths. At every point on the path, instead of checking for the conditional distribution given all the past points on the path, which is cumbersome, we consider all past points on the path within a certain distance of the current point, i.e., within a ball centered at the current point. In other words, to check the approximately-Markovian property, we evaluate $p(\gamma_{\text{SH},-0}|\gamma_{\text{SH},-1}, \gamma_{\text{SH},-2}, \ldots, \gamma_{\text{SH},-n})$ instead of $p(\gamma_{\text{SH},-0}|\gamma_{\text{SH},-1}, \gamma_{\text{SH},-2}, \ldots)$. Figure 2 (top) shows an illustration of this. This makes sense since the shadowing component has an exponential correlation function. Thus, if the radius of the ball is large enough, the points outside of the ball will have a negligible impact on the estimate at the center of the ball. We will characterize this radius in Sect. 3.2.3. Thus, our strategy is to roll a ball along the path, as shown in Fig. 2 (bottom), and to check if the approximate Markovian property holds at each point along the path. We then characterize two conditions that can ensure that a path will be approximately-Markovian. The first is that, at any point on the path, if we travel backward along the path it should not loop either within the ball or such that it re-enters the ball. We refer to such looping as d_{th}-looping (d_{th} being the radius of the ball), and examples of this are shown in Figs. 3a and 3b. Equivalently, a path is called d_{th}-loop-free if there is no d_{th}-looping. The second condition is that the maximum curvature of the path should be smaller than a certain bound, which will be characterized later in Sect. 3.2.4. If the d_{th}-loop-free condition is satisfied, then the only part of the path that lies within the ball would lie in the shaded region of Fig. 3c, and if the maximum curvature of the path is small enough, then the path will be approximately-Markovian. We will formulate this precisely in Sect. 3.2.4.

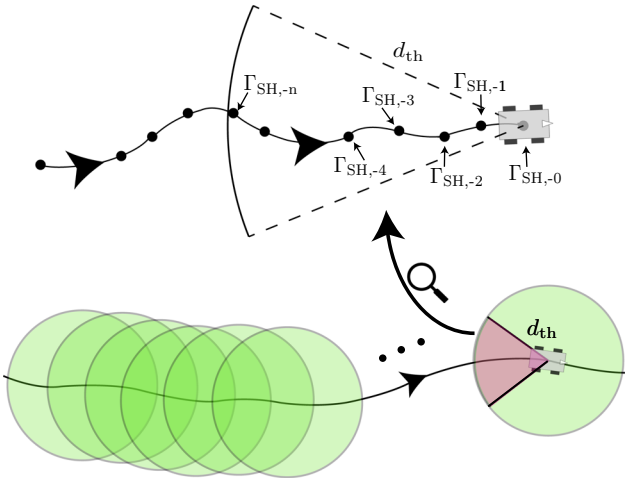

Fig. 2 (bottom) A ball with radius d_{th} rolling along the path, where we check for the approximate Markovian condition within each ball, and (top) the discretized path and the corresponding channel shadowing power values within a ball

We start by mathematically characterizing the d_{th}-looping condition in detail.

3.2.1 d_{th}-loop-free constraint

We define d_{th}-loop-free paths as paths where neither of the two following scenarios occurs at any point on the path. The first is when traveling backward along a path, the path loops within the ball itself. More precisely, when traveling backward along the path, let the initial direction of travel be along the negative x-axis. We say that the path loops within the ball

[3] Note that the discretization step size of the path must be small for the derivations of Theorem 2 to be valid.

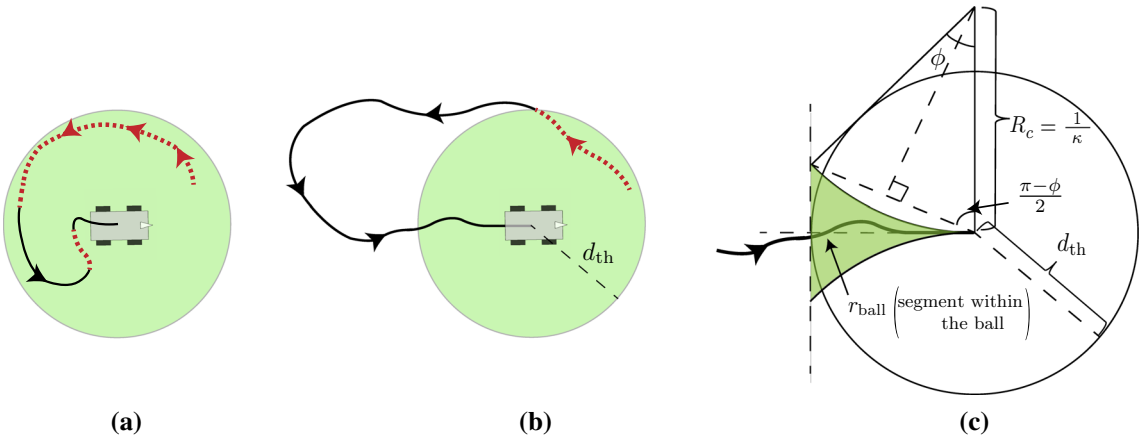

Fig. 3 **a**, **b** Two scenarios of d_{th}-looping: **a** path loops within the ball and **b** path loops back to re-enter the ball. The parts causing the loop in either scenario is denoted by the dashed red line. **c** A path of maximum curvature κ would lie within the shaded area. A sample such path is shown

if at any point (still inside the ball), the direction of travel has a component along the positive x-axis (e.g., Fig. 3a). The second scenario is when the path re-enters the ball once it leaves it. These two scenarios, which we collectively refer to as d_{th}-looping, are illustrated in Fig. 3a , b. Such d_{th}-looping behavior can possibly invalidate the approximate Markovian nature of the path.

We next relate the d_{th}-loop-free condition to the curvature of the path. We first review the precise definition of curvature.

Definition 4 *(Curvature)* (Kline 1998) The curvature of a planar path $r(s) = (x(s), y(s))$ parameterized by arc-length is defined as

$$\kappa(s) = \|T'(s)\|,$$

where $T(s)$ is the unit tangent vector at s.

When traveling backward along a path, consider the segment of the path inside the ball, before the path exits the ball. Let r_{ball} refer to this segment, as shown in Fig. 3c. Moreover, let $d_{r_{\text{ball}}}$ refer to its length. The following lemma characterizes some important properties of r_{ball}.

Lemma 2 *For a path with maximum curvature κ and a ball with radius d_{th}, the path segment r_{ball} satisfies the following properties:*

1. *r_{ball} lies within the shaded region of Fig. 3c where the boundary of the region corresponds to circular arcs with curvature κ.*
2. *If $\kappa < 1/d_{th}$, r_{ball} cannot loop within the ball (see Fig. 3a for an example of looping within the ball).*
3. *The length of the segment r_{ball} satisfies*

$$d_{r_{ball}} < \frac{1}{\kappa} \sin^{-1}(\kappa \times d_{th}).$$

Proof See "Appendix A.1" for the proof. □

Then, a sufficient condition for a d_{th}-loop-free path is given as follows.

Lemma 3 (d_{th}-loop-free path) *Consider a planar path $r(s) = (x(s), y(s))$ parameterized by arc length, i.e., s denotes the arc length. Let κ be the maximum curvature of the path. The path is d_{th}-loop-free if it satisfies $\kappa < 1/d_{th}$ and*

$$\|r(s) - r(s-d)\| > d_{th},$$

for $d > \frac{1}{\kappa} \sin^{-1}(\kappa d_{th})$ and for all s.

Proof From Lemma 2, we know that if $\kappa < 1/d_{\text{th}}$, the path cannot loop within the ball, preventing the condition of Fig. 3a. Moreover, from Lemma 2, it can easily be confirmed that $\|r(s) - r(s-d)\|$ for $d > \frac{1}{\kappa} \sin^{-1}(\kappa d_{\text{th}})$ is the euclidean distance from the center to a point on the part of the path that has left the ball. Thus, if $\|r(s) - r(s-d)\| > d_{\text{th}}$, for $d > \frac{1}{\kappa} \sin^{-1}(\kappa d_{\text{th}})$ the path cannot re-enter the ball (i.e., scenario of Fig. 3b is not possible). □

Remark 5 Any path can be reparameterized by arc length. Details on this can be found in Eberly (2008).

We next characterize the similarity or dissimilarity between the true distribution $p(\gamma_{\text{SH},-0}|\gamma_{\text{SH},-1}, \ldots, \gamma_{\text{SH},-n})$ and its Markov approximation $p(\gamma_{\text{SH},-0}|\gamma_{\text{SH},-1})$ using the KL divergence metric. We then utilize this to obtain sufficient conditions on the ball radius and the curvature of a path for the approximate Markovian nature to hold.

3.2.2 Approximately-Markovian: KL divergence metric

Consider a path as shown in Fig. 2 (top). Let $\Gamma_{\text{SH},-0}$ be the channel shadowing power on the current location and

$\Gamma_{\text{SH},-1}, \ldots, \Gamma_{\text{SH},-n}$ be the channel shadowing power on the past n locations along the path. From Sect. 2.1, we know that $\Gamma_{\text{SH},-0}, \ldots, \Gamma_{\text{SH},-n}$ are jointly Gaussian random variables. The distribution of $\Gamma_{\text{SH},-0}|\Gamma_{\text{SH},-1}, \ldots, \Gamma_{\text{SH},-n}$ is then given as $\mathcal{N}\left(m, \sigma^2\right)$, where

$$m = \Sigma_{0,1:n}^T \Sigma_{1:n}^{-1} \Gamma_{\text{SH},-1:n}, \tag{8}$$

$$\sigma^2 = \sigma_{\text{SH}}^2 - \Sigma_{0,1:n}^T \Sigma_{1:n}^{-1} \Sigma_{0,1:n}, \tag{9}$$

with $\Gamma_{\text{SH},-1:n} = [\Gamma_{\text{SH},-1}, \ldots, \Gamma_{\text{SH},-n}]^T$, $\Sigma_{0,1:n} = \mathbb{E}[\Gamma_{\text{SH},-0}\Gamma_{\text{SH},-1:n}]$ and $\Sigma_{1:n} = \mathbb{E}[\Gamma_{\text{SH},-1:n}\Gamma_{\text{SH},-1:n}^T]$ [see 10.5 of Kay (1993)]. Moreover, $\mathbb{E}[\Gamma_{\text{SH},-i}\Gamma_{\text{SH},-j}] = \sigma_{\text{SH}}^2 e^{-\|q_i - q_j\|/\beta_{\text{SH}}}$, where $q_i \in \mathbb{R}^2$ is the location corresponding to $\Gamma_{\text{SH},-i}$. Let $\alpha = \Sigma_{1:n}^{-1}\Sigma_{0,1:n}$ denote the coefficients of the mean. We then have $m = \alpha^T \Gamma_{\text{SH},-1:n} = \alpha_1\Gamma_{\text{SH},-1} + \ldots + \alpha_n\Gamma_{\text{SH},-n}$.

We want to approximate this distribution with the Markovian distribution $\Gamma_{\text{SH},-0}|\Gamma_{\text{SH},-1} \sim \mathcal{N}\left(\hat{m}, \hat{\sigma}^2\right)$ where $\hat{m} = \rho\Gamma_{\text{SH},-1}$ and $\hat{\sigma}^2 = \sigma_{\text{SH}}^2(1-\rho^2)$, with $\rho = e^{-\Delta d/\beta_{\text{SH}}}$, and Δd being the step size of the path. We first characterize the difference between the means, given as $\Delta m = m - \hat{m} = \Delta\alpha^T \Gamma_{\text{SH},-1:n}$, where $\Delta\alpha = [\alpha_1 - \rho, \alpha_2, \ldots, \alpha_n]^T$. Δm is thus a zero-mean Gaussian random variable $\mathcal{N}\left(0, \sigma_{\Delta m}^2\right)$, where

$$\sigma_{\Delta m}^2 = \Delta\alpha^T \Sigma_{1:n} \Delta\alpha. \tag{10}$$

We will compare how close the true distribution and its approximation are using the KL divergence metric. We first review the definition of KL divergence.

Definition 5 *(KL Divergence)* (Cover and Thomas 2012) The KL divergence between two distributions $p(x)$ and $\tilde{p}(x)$ is defined as

$$KL = \int p(x) \log_e \frac{p(x)}{\tilde{p}(x)} dx.$$

KL divergence is a measure of the distance between two distributions (Cover and Thomas 2012). We will utilize this as a measure of the goodness of the approximation: the smaller the KL divergence, the better the approximation. The following lemma gives us the expression for this KL divergence.

Lemma 4 *The KL divergence between $\mathcal{N}(m, \sigma^2)$ and its approximation $\mathcal{N}(\hat{m}, \hat{\sigma}^2)$ is given as*

$$KL = \frac{\sigma_{\Delta m}^2}{2\hat{\sigma}^2}\chi_1^2 + \frac{1}{2}\left(\frac{\sigma^2}{\hat{\sigma}^2} - 1 - \log_e \frac{\sigma^2}{\hat{\sigma}^2}\right), \tag{11}$$

where $\chi_1^2 = (m - \hat{m})^2/\sigma_{\Delta m}^2$.

Proof See Robert (1996) for the proof. □

Since m and $\hat{m}$ are functions of $\Gamma_{\text{SH},-1}, \ldots, \Gamma_{\text{SH},-n}$, they are random variables. Thus, χ_1^2 becomes a Chi-squared random variable with one degree of freedom since $(m - \hat{m}) \sim (0, \sigma_{\Delta m}^2)$ (Lancaster and Seneta 2005), and the KL divergence of (11) becomes a random variable. More specifically, from (11), we know that the KL divergence is a scaled Chi-squared random variable with an offset term. We use the mean m_{KL} and the standard deviation σ_{KL} of the KL divergence to capture the deviation of the Markov approximation from the true distribution. The smaller these values are, the better the approximation is. In our approach, we set maximum tolerable values for the mean and the standard deviation as ϵ_m and ϵ_σ respectively. Then, we say that the distribution is approximately-Markovian for the parameters ϵ_m and ϵ_σ if we satisfy $m_{KL} \leq \epsilon_m$ and $\sigma_{KL} \leq \epsilon_\sigma$.

We next consider the setting with 3 points in space, as shown in Fig. 4a, where we have the current point ($\Gamma_{\text{SH},-0}$), the previous point ($\Gamma_{\text{SH},-1}$) and a general point in space ($\Gamma_{\text{SH},r}$). We are interested in mathematically characterizing the impact of $\Gamma_{\text{SH},r}$ on the estimate at the current point, i.e., how good an approximation $\Gamma_{\text{SH},-0}|\Gamma_{\text{SH},-1} \sim \mathcal{N}(\hat{m}, \hat{\sigma}^2)$ is for the true distribution $\Gamma_{\text{SH},-0}|\Gamma_{\text{SH},-1}, \Gamma_{\text{SH},r} \sim \mathcal{N}(m, \sigma^2)$. As we shall see, we will utilize this analysis in such a way that it serves as a good proxy for the general n point analysis. Specifically, we will utilize it to obtain bounds on the ball radius as well as on the maximum allowed curvature of a path in Sects. 3.2.3 and 3.2.4 respectively. Let $d_1 = \|q_0 - q_1\|$, $d_r = \|q_0 - q_r\|$, and $d_{1r} = \|q_1 - q_r\|$, as shown in Fig. 4a,

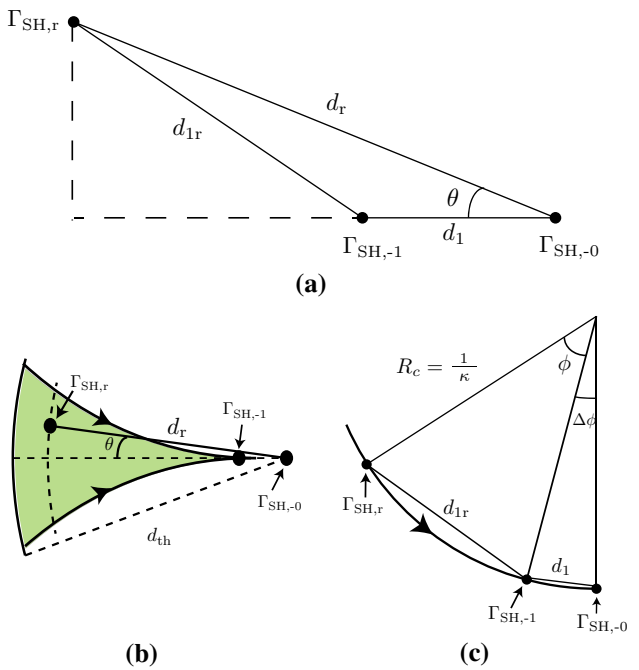

Fig. 4 3 points analysis **a** for a general case, **b** for a path with maximum curvature κ that satisfies $\kappa < 1/d_{\text{th}}$, and **c** along a path with a constant curvature

where q_r is the location of the general point. Moreover, $d_1 = \Delta d$.

The following lemma characterizes the mean and standard deviation of the KL divergence between the true distribution and its approximation for the 3 point analysis.

Lemma 5 *The mean and standard deviation of the KL divergence between the true distribution $\mathcal{N}(m, \sigma^2)$ and its approximation $\mathcal{N}(\hat{m}, \hat{\sigma}^2)$ for the 3 point analysis of Fig. 4a is given as*

$$m_{KL} = -\frac{1}{2}\log_e\left(1 - \frac{\sigma_{\Delta m}^2}{\hat{\sigma}^2}\right),$$

$$\sigma_{KL} = \frac{\sigma_{\Delta m}^2}{\sqrt{2}\hat{\sigma}^2},$$

where

$$\sigma_{\Delta m}^2 = \sigma_{SH}^2 \frac{\left(e^{-d_r/\beta_{SH}} - e^{-(d_1+d_{1r})/\beta_{SH}}\right)^2}{1 - e^{-2d_{1r}/\beta_{SH}}}.$$

Proof See "Appendix A.2" for the proof. □

Any point on the path can belong to three possible regions: (1) the shaded region within the ball of Fig. 3c, (2) within the ball but outside the shaded region, and (3) outside the ball. If the path is d_{th}-loop-free, then no point of the path lies within region 2 (i.e., within the ball but outside the shaded region). We next characterize the minimum ball radius and the maximum allowed curvature of a path such that the impact of any point ($\Gamma_{\text{SH},r}$) in region 1 and 3 on the estimate at the center of the ball is negligible.

3.2.3 Ball radius

We next utilize our analysis to determine the ball radius d_{th}. We wish to select the minimum d_{th} such that the impact of any point outside the ball on the approximation is within the tolerable KL divergence parameters ϵ_m and ϵ_σ, i.e., the KL divergence between the true and the approximating distribution (in the 3 point analysis) satisfies $m_{KL} \leq \epsilon_m$ and $\sigma_{KL} \leq \epsilon_\sigma$.

The following lemma characterizes what the minimum ball radius d_{th} should be.

Lemma 6 *The minimum ball radius d_{th} such that any point outside the ball satisfies the maximum tolerable KL divergence parameters ϵ_m and ϵ_σ for the 3 point analysis, is given by*

$$d_{th} = \frac{\beta_{SH}}{2}\log_e\left(\rho^2 + \frac{1-\rho^2}{\epsilon_d}\right),$$

where $\rho = e^{-\Delta d/\beta_{SH}}$ and $\epsilon_d = \min\left\{1 - e^{-2\epsilon_m}, \sqrt{2}\epsilon_\sigma\right\}$.

Proof See "Appendix A.3" for the proof. □

3.2.4 Curvature constraint

We next utilize the 3 point analysis to determine the maximum curvature of a path such that it is approximately-Markovian, i.e., it satisfies the KL divergence constraint $m_{KL} \leq \epsilon_m$ and $\sigma_{KL} \leq \epsilon_\sigma$.

Consider the scenario in Fig. 4b. For a given maximum curvature κ, any valid point of the path must lie within the shaded region of the figure, where the boundary corresponds to circular paths with curvature κ. We wish to find the maximum allowed curvature such that the impact of any point within the shaded region on the approximation is within the tolerable KL divergence parameters ϵ_m and ϵ_σ, i.e., the KL divergence between the true and the approximating distribution (in the 3 point analysis) satisfies $m_{KL} \leq \epsilon_m$ and $\sigma_{KL} \leq \epsilon_\sigma$. The following lemma characterizes this maximum allowed curvature as the solution of an optimization problem.

Lemma 7 *The maximum allowed curvature κ_{th} such that any past point on the path within the ball of radius d_{th} satisfies the maximum tolerable KL divergence parameters ϵ_m and ϵ_σ for the 3 point analysis, is the solution to the following optimization problem:*

$$\begin{aligned} &\textit{maximize } \kappa \\ &\textit{subject to } \max_{\phi:0<\phi\leq h_{cons}(\kappa)} h_{opt}(\kappa,\phi) \leq \epsilon_d \\ &\qquad\qquad \kappa < 1/d_{th}, \end{aligned} \tag{12}$$

where

$$h_{opt}(\kappa,\phi) = \frac{\left(e^{-\frac{2}{\kappa\beta_{SH}}\sin(\frac{\phi+\Delta\phi}{2})} - \rho e^{-\frac{2}{\kappa\beta_{SH}}\sin(\frac{\phi}{2})}\right)^2}{(1 - e^{-\frac{4}{\kappa\beta_{SH}}\sin(\frac{\phi}{2})})(1-\rho^2)},$$

and $h_{cons}(\kappa) = 2\sin^{-1}(\frac{\kappa d_{th}}{2}) - \Delta\phi$, $\Delta\phi = 2\sin^{-1}(\frac{\kappa\Delta d}{2})$, $\rho = e^{-\Delta d/\beta_{SH}}$, $\epsilon_d = \min\left\{1 - e^{-2\epsilon_m}, \sqrt{2}\epsilon_\sigma\right\}$.

Proof See "Appendix A.4" for the proof. □

Remark 6 Ideally, we would have preferred to use the KL divergence between the approximation and the true distribution where we condition on all the past points on the path within the ball radius, as opposed to using just the point with the maximal impact. However, such an analysis does not lend itself to a neat characterization of the maximum allowed curvature. Through simulations, we have seen that the 3 point analysis, as described in Lemma 7, serves as a good proxy for the n past points case on a circular path (which has a maximum curvature everywhere for a given κ). For instance, for parameters $\kappa = 1/15$, $\Delta d = 0.1$ and

$\beta_{\text{SH}} = 5$ m, the KL divergence mean and standard deviation when considering all the past points of the path within the ball are $m_{KL} = 6 \times 10^{-7}$ and $\sigma_{KL} = 9 \times 10^{-7}$ respectively. This is comparable (in terms of the order of magnitude) to the values $m_{KL} = 3 \times 10^{-7}$ and $\sigma_{KL} = 5 \times 10^{-7}$ obtained for the 3 point analysis from Lemma 7.

Finally, we put together all our results to provide sufficient conditions for an approximately-Markovian path.

Lemma 8 (Approximately-Markovian path) *Let $r(s) = (x(s), y(s))$ be a path parameterized by its arc length. The path is approximately-Markovian for given maximum tolerable KL divergence parameters ϵ_m and ϵ_σ for the 3 point analysis, if it satisfies the following conditions:*

1. *$r(s)$ is d_{th}-loop-free for ball radius d_{th} (as characterized by Lemma 3),*
2. *curvature $\kappa(s) < \kappa_{th}$ for all s,*

where d_{th} and κ_{th} are obtained from Lemmas 6 and 7 respectively.

Consider a given path. For a given ϵ_m and ϵ_σ, we can check if the path satisfies the conditions of Lemma 8. If it does, we can then directly use the results of Sect. 3.1 to obtain the PDF of the FPD for the path. Note that even if the path does not satisfy the conditions, the path may still be approximately-Markovian as the conditions of Lemma 8 are sufficient conditions.

4 Characterizing FPD considering multipath

The previous section analyzed the FPD to the connectivity threshold when the multipath component was ignored. In this section, we show how to derive the FPD density in the presence of the multipath fading component, and for the most general channel model of $\Gamma(d) = \gamma_{\text{PL}}(d) + \Gamma_{\text{SH}}(d) + \Gamma_{\text{MP}}(d)$. We begin by analyzing straight paths in Sect. 4.1, where we derive the PDF of the FPD using a recursive formulation. We then extend our analysis to a larger space of paths in Sect. 4.2.

4.1 Straight paths: a recursive characterization

We first characterize the PDF of the distance traveled until connectivity for straight paths. We consider the scenario described in Sect. 3.1, where a robot situated at a distance d_{src} from a remote operator to which it needs to be connected, moves in a straight path in the direction specified by the angle θ_{src}, as shown in Fig. 1b. $\Gamma(d)$ represents the channel power when the robot is at distance d along direction θ_{src}, as marked in Fig. 1b.

Recall that we define connectivity as the event where $\Gamma(d) \geq \gamma_{\text{th}}$. The connectivity requirement is then given as $\Gamma(d) = \gamma_{\text{PL}}(d) + \Gamma_{\text{SH}}(d) + \Gamma_{\text{MP}}(d) \geq \gamma_{\text{th}}$, considering all the channel components. In this case, the approach of Sect. 3.1 is not applicable anymore as we no longer deal with a Markov process. Even if the multipath component was taken to be a Gauss–Markov process [which could be a valid model for some environments (Hashemi 1994), the resultant channel power would not be Markovian, as can be verified from Lemma 1. In this section, we assume that the robot measures the channel along the chosen straight path in discrete steps of size Δd. We assume that Δd is such that the multipath random variable is uncorrelated at the distance Δd apart [this is a realistic assumption as multipath decorrelates fast (Malmirchegini and Mostofi 2012)]. We then index the channel power and shadowing components accordingly, i.e., let $\Gamma_k = \Gamma(k\Delta d)$ and $\Gamma_{\text{SH},k} = \Gamma_{\text{SH}}(k\Delta d)$. The probability of failure of connectivity at the end of N steps (given the initial failure of connectivity) can then be written as

$$\Pr(\Gamma_1, \Gamma_2, \ldots, \Gamma_N < \gamma_{\text{th}} | \Gamma_0 < \gamma_{\text{th}}) = \int_{\gamma_1, \ldots, \gamma_N < \gamma_{\text{th}}} \cdots \int p(\gamma_1, \ldots, \gamma_N | \Gamma_0 < \gamma_{\text{th}}) \mathrm{d}\gamma_1 \ldots \mathrm{d}\gamma_N, \quad (13)$$

where $p(\gamma_1, \ldots, \gamma_N | \Gamma_0 < \gamma_{\text{th}})$ is the conditional joint density function of $\Gamma_1, \ldots, \Gamma_N$. Consider the computation of this integral, which is an integration in an N dimensional space. If we discretize the domain of Γ_k into M parts, then a direct computation of the FPD for up to N steps would have a computational complexity of $O(NM^N)$, which is infeasible for high values of M and N. Instead, we show how this can be solved efficiently through a recursive integral computation in $O(NM\log(M))$. In contrast, our previously proposed dynamic programming approach of Muralidharan and Mostofi (2017b) had a computational complexity of $O(N^2M^2)$.

As mentioned before, the robot measures the channel in discrete steps of size Δd. Let $d_k = k\Delta d$ denote the distance when k steps are taken. Then, it can be shown, using (2), that the shadowing component is an autoregressive AR(1) process, the continuous analogue of which is the Ornstein–Uhlenbeck process (note that the shadowing component is Markovian):

$$\Gamma_{\text{SH},k+1} = \rho\Gamma_{\text{SH},k} + \sigma_{\text{SH}}\sqrt{1-\rho^2}Z_k,$$

where $\rho = e^{-\Delta d/\beta_{\text{SH}}}$ and Z_k are i.i.d. with a standard normal distribution. The conditional random variable $\Gamma_{\text{SH},k+1}|\gamma_{\text{SH},k}$ is thus a Gaussian random variable with mean $\rho\gamma_{\text{SH},k}$ and variance $\sigma^2_{\text{SH}}(1-\rho^2)$.

Note that the desired probability of (13) can be expressed as

$$\Pr\left(\Gamma_1,\ldots,\Gamma_N<\gamma_{\text{th}}|\Gamma_0<\gamma_{\text{th}}\right)=\frac{\Pr\left(\Gamma_0,\ldots,\Gamma_N<\gamma_{\text{th}}\right)}{\Pr\left(\Gamma_0<\gamma_{\text{th}}\right)}. \tag{14}$$

We next show how to compute $\Pr(\Gamma_0,\Gamma_1,\ldots\Gamma_N<\gamma_{\text{th}})$ via a recursive characterization. This is inspired in part by the calculation of orthant probabilities for auto-regressive sequences in Craig (2008). Define the set of functions $\mathcal{J}_k$, as follows:

$$\begin{aligned}\mathcal{J}_k(\gamma_{\text{SH},k})=&\int_{\gamma_{\text{MP},k}=-\infty}^{\gamma_{\text{th}}-\gamma_{\text{PL}}(d_k)-\gamma_{\text{SH},k}}\\&\times\int_{S_{k-1}}\cdots\int p(\gamma_{\text{SH},0},\gamma_{\text{MP},0},\ldots,\gamma_{\text{SH},k},\gamma_{\text{MP},k})\\&\times\mathrm{d}\gamma_{\text{SH},0}\mathrm{d}\gamma_{\text{MP},0}\ldots\mathrm{d}\gamma_{\text{SH},k-1}\mathrm{d}\gamma_{\text{MP},k-1}\mathrm{d}\gamma_{\text{MP},k}\end{aligned} \tag{15}$$

where $S_{k-1}=\cap_{i=0}^{k-1}\{\gamma_{\text{SH},i},\gamma_{\text{MP},i}:\gamma_{\text{PL}}(d_i)+\gamma_{\text{SH},i}+\gamma_{\text{MP},i}<\gamma_{\text{th}}\}$ and $p(\gamma_{\text{SH},0},\gamma_{\text{MP},0},\ldots,\gamma_{\text{SH},k},\gamma_{\text{MP},k})$ is the joint density of $\Gamma_{\text{SH},0},\Gamma_{\text{MP},0},\ldots,\Gamma_{\text{SH},k},\Gamma_{\text{MP},k}$. Note that

$$\begin{aligned}&\Pr\left(\Gamma_0,\Gamma_1,\ldots,\Gamma_N<\gamma_{\text{th}}\right)\\&=\int_{S^N}\cdots\int p(\gamma_{\text{SH},0},\gamma_{\text{MP},0},\ldots,\gamma_{\text{SH},N},\gamma_{\text{MP},N})\\&\quad\times\mathrm{d}\gamma_{\text{SH},0}\mathrm{d}\gamma_{\text{MP},0}\ldots\mathrm{d}\gamma_{\text{SH},N}\mathrm{d}\gamma_{\text{MP},N}\\&=\int_{\gamma_{\text{SH},N}=-\infty}^{\infty}\mathcal{J}_N(\gamma_{\text{SH},N})\mathrm{d}\gamma_{\text{SH},N}.\end{aligned} \tag{16}$$

In the following lemma we show how to compute $\mathcal{J}_k(\gamma_{\text{SH},k})$ recursively.

Lemma 9 *The functions $\mathcal{J}_k$, for $k=1,\ldots,N$, of (15) can be computed by the recursion:*

$$\begin{aligned}\mathcal{J}_{k+1}(\gamma_{SH,k+1})=&F_{MP}(\gamma_{th}-\gamma_{PL}(d_{k+1})-\gamma_{SH,k+1})\\&\times\frac{1}{\rho}\int_{u=-\infty}^{\infty}\varphi\left(\frac{\gamma_{SH,k+1}-u}{\sigma_{SH}\sqrt{1-\rho}}\right)\mathcal{J}_k\left(\frac{u}{\rho}\right)\mathrm{d}u,\end{aligned}$$

initialized with

$$\mathcal{J}_0(\gamma_{SH,0})=F_{MP}(\gamma_{th}-\gamma_{PL}(0)-\gamma_{SH,0})\varphi\left(\frac{\gamma_{SH,0}}{\sigma_{SH}}\right),$$

where $F_{MP}(.)$ is the CDF of the multipath random variable Γ_{MP} and $\varphi(.)$ is the standard Gaussian density function.

Proof It can be seen that this clearly holds for $k=0$:

$$\begin{aligned}\mathcal{J}_0(\gamma_{\text{SH},0})&=\int_{\gamma_{\text{MP},k}=-\infty}^{\gamma_{\text{th}}-\gamma_{\text{PL}}(d_0)-\gamma_{\text{SH},0}}p(\gamma_{\text{SH},0},\gamma_{\text{MP},0})\mathrm{d}\gamma_{\text{MP},0}\\&=F_{\text{MP}}(\gamma_{\text{th}}-\gamma_{\text{PL}}(0)-\gamma_{\text{SH},0})\varphi\left(\frac{\gamma_{\text{SH},0}}{\sigma_{\text{SH}}}\right).\end{aligned}$$

Next, $\mathcal{J}_{k+1}(\gamma_{\text{SH},k+1})$ can be expanded as

$$\begin{aligned}&\mathcal{J}_{k+1}(\gamma_{\text{SH},k+1})\\&=\int_{-\infty}^{\gamma_{\text{th,MP},k+1}}\int_{S_k}\cdots\int p(\gamma_{\text{SH},0},\gamma_{\text{MP},0},\ldots,\gamma_{\text{SH},k+1},\gamma_{\text{MP},k+1})\\&\quad\times\mathrm{d}\gamma_{\text{SH},0}\mathrm{d}\gamma_{\text{MP},0}\ldots\mathrm{d}\gamma_{\text{SH},k}\mathrm{d}\gamma_{\text{MP},k}\mathrm{d}\gamma_{\text{MP},k+1}\\&=\int_{-\infty}^{\gamma_{\text{th,MP},k+1}}p(\gamma_{\text{MP},k+1})\mathrm{d}\gamma_{\text{MP},k+1}\int_{-\infty}^{\infty}p(\gamma_{\text{SH},k+1}|\gamma_{\text{SH},k})\\&\quad\times\int_{-\infty}^{\gamma_{\text{th,MP},k}}\int_{S_{k-1}}\cdots\int p(\gamma_{\text{SH},0},\gamma_{\text{MP},0},\ldots,\gamma_{\text{SH},k},\gamma_{\text{MP},k})\\&\quad\times\mathrm{d}\gamma_{\text{SH},0}\mathrm{d}\gamma_{\text{MP},0}\ldots\mathrm{d}\gamma_{\text{SH},k-1}\mathrm{d}\gamma_{\text{MP},k-1}\mathrm{d}\gamma_{\text{MP},k}\\&=F_{\text{MP}}(\gamma_{\text{th,MP},k+1})\\&\quad\times\int_{-\infty}^{\infty}\varphi\left(\frac{\gamma_{\text{SH},k+1}-\rho\gamma_{\text{SH},k}}{\sigma_{\text{SH}}\sqrt{1-\rho}}\right)\mathcal{J}_k(\gamma_{\text{SH},k})\mathrm{d}\gamma_{\text{SH},k}\\&=\frac{F_{\text{MP}}(\gamma_{\text{th,MP},k+1})}{\rho}\int_{u=-\infty}^{\infty}\varphi\left(\frac{\gamma_{\text{SH},k+1}-u}{\sigma_{\text{SH}}\sqrt{1-\rho}}\right)\mathcal{J}_k\left(\frac{u}{\rho}\right)\mathrm{d}u,\end{aligned}$$

where $\gamma_{\text{th,MP},k}=\gamma_{\text{th}}-\gamma_{\text{PL}}(d)-\gamma_{\text{SH},k}$. □

Remark 7 Note that the recursive integral in Lemma 9 is in the form of a convolution. This can be computed efficiently using the Fast Fourier transform.

Using Lemma 9, we can compute $\Pr\left(\Gamma_0,\Gamma_1,\ldots,\Gamma_N<\gamma_{\text{th}}\right)$ as shown in (16), which in turn is used to compute $\Pr\left(\Gamma_1,\ldots\Gamma_N<\gamma_{\text{th}}|\Gamma_0<\gamma_{\text{th}}\right)$ via (14).

Next, we use this result to calculate the FPD probability. Let $\mathcal{K}=\min_{k=1,2,\ldots}\{k:\Gamma_k\geq\gamma_{\text{th}},\Gamma_0<\gamma_{\text{th}}\}$ be the random variable which denotes the upcrossing first passage step to connectivity given that Γ_0 is restricted to lie below γ_{th}. Then,

$$\begin{aligned}\Pr(\mathcal{K}=k)&=\Pr\left(\Gamma_1,\ldots\Gamma_{k-1}<\gamma_{\text{th}},\Gamma_k\geq\gamma_{\text{th}}|\Gamma_0<\gamma_{\text{th}}\right)\\&=\Pr\left(\Gamma_1,\ldots\Gamma_{k-1}<\gamma_{\text{th}}|\Gamma_0<\gamma_{\text{th}}\right)\\&\quad-\Pr\left(\Gamma_1,\ldots\Gamma_k<\gamma_{\text{th}}|\Gamma_0<\gamma_{\text{th}}\right),\end{aligned}$$

where both terms on the right hand side can be obtained from our recursive characterization using Lemma 9.

4.2 Approximately-Markovian paths

As we saw in Sect. 4.1, we can compute the PDF of the FPD for straight paths when considering multipath, using Lemma 9, which provides a low complexity recursive method to do so. This recursive characterization of Lemma 9 depends on the channel shadowing power being a Markov process. Specifically, the proof of Lemma 9 requires that $p(\gamma_{\text{SH},-0}|\gamma_{\text{SH},-1},\gamma_{\text{SH},-2},\ldots)=p(\gamma_{\text{SH},-0}|\gamma_{\text{SH},-1})$, where $\Gamma_{\text{SH},-0}$ is the shadowing power at the current location and

$\Gamma_{\text{SH},-1}, \Gamma_{\text{SH},-2}, \ldots$ are the channel shadowing power at previously visited points, as shown in Fig. 2 (top). As a result, Lemma 9 can be applied to approximately-Markovian paths as defined in Sect. 3.2. More specifically, we can use Lemma 8 to determine whether a path is approximately-Markovian for given maximum tolerable KL divergence parameters ϵ_m and ϵ_σ. We can then obtain the statistics of the FPD for such an approximately-Markovian path in multipath environments using Lemma 9.

Remark 8 (Computational complexity) A natural question that arises is: *why not use the results of Sect. 4.1 to tackle the case without considering multipath of Sect. 3.1*? We next address this. As discussed in Sect. 4.1, the computation cost of Lemma 9 for up to N steps is $O(NM\log(M))$. In contrast, the computational cost of Theorem 2 for the case without considering multipath, for up to N steps, is $O(N^2)$. Since $M \gg N$, the stochastic differential equation approach is more computationally efficient. Moreover, the characterization of the ϵ-upcrossing FPD of Sect. 3.1 can be used for analytical purposes.

Remark 9 Several paths satisfy the approximately-Markovian conditions. In Sect. 5, we will see examples of logarithmic spirals and archimedian spirals that are approximately-Markovian. More than the type of the path, it is the parameters of the path that determine whether it will satisfy the approximate-Markovian conditions of Lemma 8. For instance, even a circular path segment with a small enough curvature, which ends before completing the loop, can be approximately-Markovian. More generally, any path that does not have sharp turns (i.e., has small curvature) and which does not loop would be approximately-Markovian.

5 Numerical results based on real channel data

In this section, we validate the derivations of Sects. 3 and 4 in a simulation environment with real channel parameters from two different channel environments. We also highlight interesting trends of the FPD statistics as a function of the channel parameters. The channel is generated using the channel model described in Sect. 2.1, with parameters obtained from real channel measurements in downtown San Francisco (Smith and Cox 2004). More specifically, we consider two sets of channel parameters which are obtained from real channel measurements collected in two different channel environments (regions) in downtown San Francisco: Sansome street and California street. Figure 5 shows real received signal measurements in both regions. The channel parameters for Sansome street are: $n_{\text{PL}} = 4.2$, $\sigma^2_{\text{SH}} = 8.41$, and $\beta_{\text{SH}} = 12.92$ m. The channel parameters for California street are: $n_{\text{PL}} = 6.3$, $\sigma^2_{\text{SH}} = 7.84$, and $\beta_{\text{SH}} = 3.06$ m.

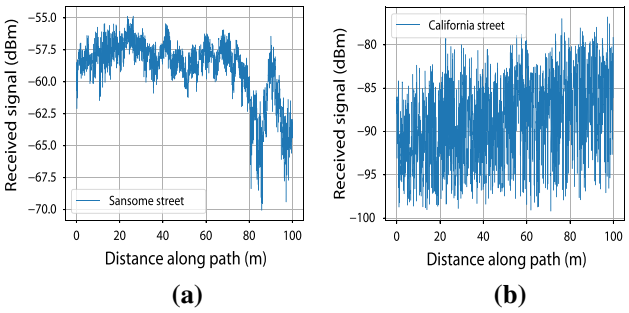

Fig. 5 Real channel measurements in two different channel environments in downtown San Francisco: **a** Sansome street, and **b** California street

We impose a minimum required received SNR of 20 dB, the noise power is taken to be a realistic −100 dBmW, and the transmit power is taken to be 30 dBmW, which results in a channel power connectivity threshold of $\gamma_{\text{th}} = -110$ dB. We furthermore take the upcrossing FPD constant to be $\epsilon = 0.1$ in the simulation results.

We consider a discretization step size of $\Delta d = 0.03$ m. Let the maximum tolerable KL divergence parameters be $\epsilon_m = 0.001$ and $\epsilon_\sigma = 0.001$. Then, the ball radius $d_{\text{th}} = 9.5$ m and the maximum allowed curvature $\kappa_{\text{th}} = 0.104$ m^{-1} satisfy Lemmas 6 and 7 respectively for both channel environments. We will demonstrate the efficacy of our proposed approaches through three different paths that satisfy these constraints and are thus approximately-Markovian: (1) an archimedian spiral with equation $r_d = 11 + 5e^{\theta}$, (2) a logarithmic spiral with equation $r_d = 11e^{0.5\theta}$, and (3) a straight path where the robot moves straight towards the remote station (i.e., $\theta_{\text{src}} = 0$ rad), where both the spiral equations are in polar coordinates (r_d, θ). Figure 6a, b show the path and the curvature along the path of the archimedian spiral respectively, Fig. 6c, d show the path and the curvature along the path of the logarithmic spiral respectively, and Fig. 6e, f show the path and the curvature along the straight path respectively. The remote station is located at the origin as denoted in Fig. 6a, c, e. We run simulations for these three robotic paths in the two different channel environments, i.e., using the channel parameters from Sansome street and California street. The paths considered for the Sansome street simulations are as shown in Fig. 6, where the initial location of the robot is at a distance of 450 m. The paths for the California street simulations are the same, except that the initial location of the robot is at a distance of 600 m.

5.1 Results without considering multipath

We first consider the case without multipath. Figure 7a–f show the statistics of the upcrossing FPD for the Sansome street channel parameters. More specifically, Fig. 7a, b show the PDF and CDF of the upcrossing FPD for the archime-

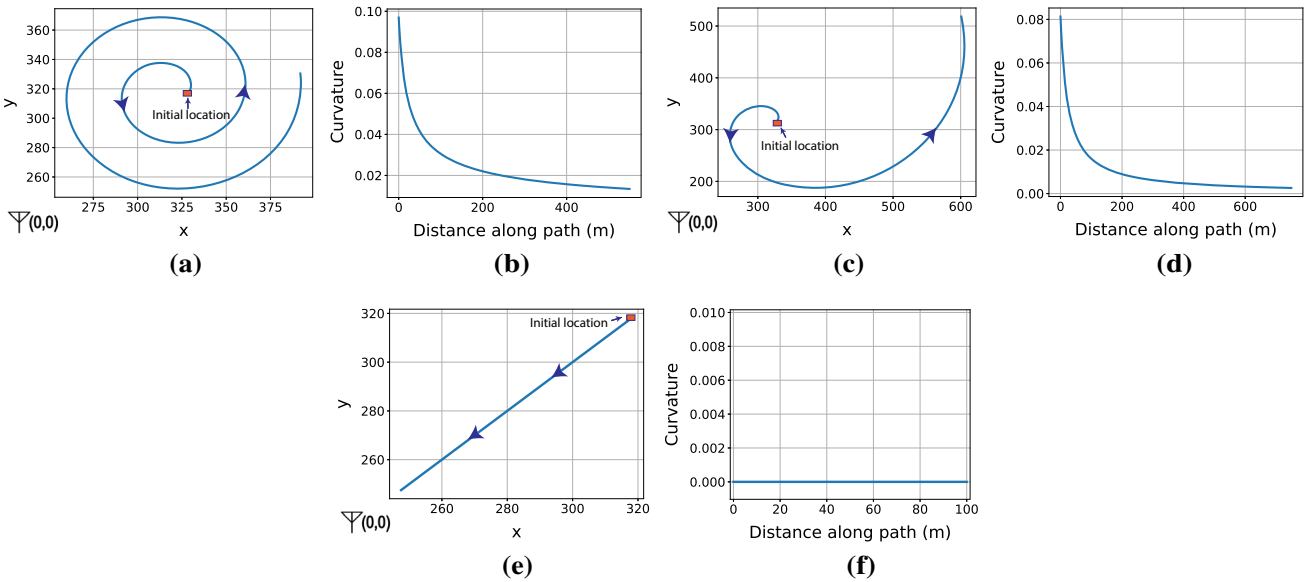

Fig. 6 Path followed by the robot and the curvature along the path for **a**, **b** the archimedian spiral, **c**, **d** the logarithmic spiral, and **e**, **f** the straight path

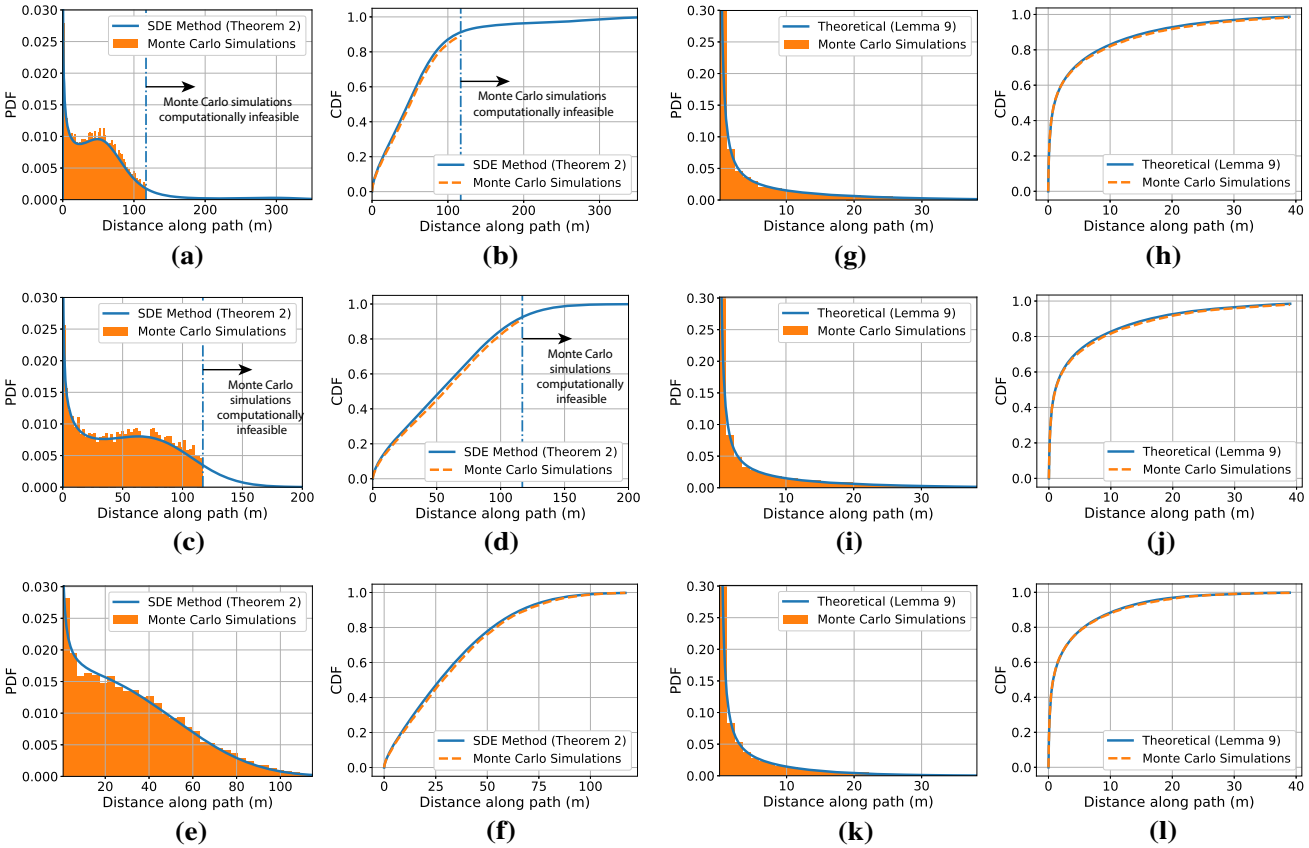

Fig. 7 Simulations for the Sansome street channel parameters: PDF and CDF of upcrossing FPD without considering multipath for **a**, **b** the archimedian spiral, **c**, **d** the logarithmic spiral, and **e**, **f** the straight path. PDF and CDF of upcrossing FPD when including multipath for **g**, **h** the archimedian spiral, **i**, **j** the logarithmic spiral, and **k**, **l** the straight path

dian path respectively, Fig. 7c, d show the PDF and CDF of the upcrossing FPD for the logarithmic path respectively, and Fig. 7e, f show the PDF and CDF of the upcrossing FPD for the straight path respectively. We can see that, for all three paths, our theoretical derivations match the true statistics obtained via Monte Carlo simulations very well, where we simulate the channel along the path 10, 000 times. Similarly, Fig. 8a, f show the PDF and CDF of the upcrossing FPD for all three paths for the California street channel parameters. We can see that our theoretical derivations match the true statistics obtained via Monte Carlo simulations very well.

5.2 Results when including multipath

Next, consider the case where multipath of the environment can not be neglected. We then simulate the multipath fading as an uncorrelated Rician random variable. Rician distribution is a common distribution for characterizing multipath (Rappaport 1996) and is given by

$$f_{\text{ric}}(z) = (1 + K_{\text{ric}})e^{-K_{\text{ric}}-(1+K_{\text{ric}})z} I_0\left(2\sqrt{zK_{\text{ric}}(1 + K_{\text{ric}})}\right),$$

where $I_0(.)$ is the modified 0th order Bessel function and the parameter K_{ric} is the ratio of the power in the line of sight component to the power in the non-line of sight components of the channel. We use the Rician parameter which we obtain from the real channel measurements in downtown San Francisco: $K_{\text{ric}} = 1.59$ for the Sansome street scenario, and $K_{\text{ric}} = 3.16$ for the California street scenario. We further assume that the multipath component gets uncorrelated at our discretization interval of 0.03 m, which is a reasonable assumption in many cases (Malmirchegini and Mostofi 2012).

Figure 7g–l show the statistics of the upcrossing FPD, when including multipath, for the Sansome street channel parameters. Figure 7g, h show the PDF and CDF of the upcrossing FPD for the archimedian path respectively, Fig. 7i, j show the PDF and CDF of the upcrossing FPD for the logarithmic path respectively, and Fig. 7k, l show the PDF and CDF of the upcrossing FPD for the straight path respectively. The histogram obtained via Monte Carlo simulations is also plotted for comparison, where we simulate the channel along the path 10, 000 times. It can be seen that in the case of all three paths, our derivations match the true

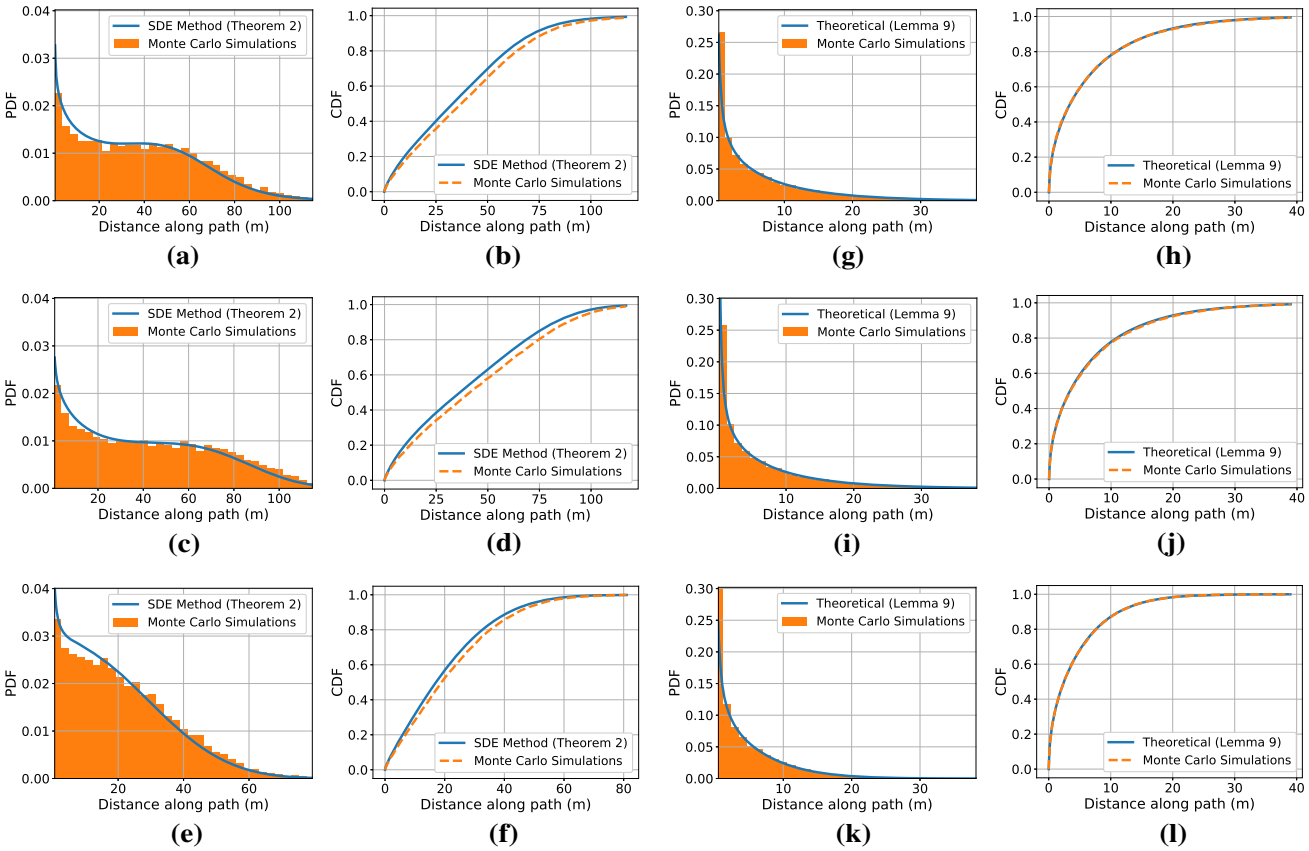

Fig. 8 Simulations for the California street channel parameters: PDF and CDF of upcrossing FPD without considering multipath for **a**, **b** the archimedian spiral, **c**, **d** the logarithmic spiral, and **e**, **f** the straight path. PDF and CDF of upcrossing FPD when including multipath for **g**, **h** the archimedian spiral, **i**, **j** the logarithmic spiral, and **k**, **l** the straight path

statistics very well. Similarly, Fig. 8g–l show the PDF and CDF of the upcrossing FPD for all three paths for the California street channel parameters. We can see that our theoretical derivations match the true statistics obtained via Monte Carlo simulations very well.

Finally, different environments will have different underlying channel parameters. Thus, we next consider the impact of the underlying channel parameters on the FPD. Figure 9a, b show the expected distance traveled as a function of the shadowing decorrelation distance (β_{SH}) and the shadowing variance (σ^2_{SH}) respectively when $d_{\text{src}} = 550$ m and $\theta_{\text{src}} = 0$ rad, along a straight path. The channel parameters, except for the parameter being varied, are fixed at the Sansome street channel parameters. Increasing the shadowing power directly increases the spatial variance of the channel power. Thus, with a higher probability, $\Gamma(d)$ stumbles upon the connectivity threshold earlier, resulting in a smaller FPD, as can be seen. An increase in the decorrelation distance, on the other hand, implies a greater spatial correlation of the channel power and decreases the spatial variation. Thus, we observe that the expected traveled distance increases when increasing the decorrelation distance. Figure 9c shows the expected distance until connectivity as a function of K_{ric} of multipath. For large values of K_{ric}, the line of sight component dominates and results in a more deterministic multipath term. Decreasing K_{ric}, on the other hand, results in an increase in the variance of the multipath component, thus increasing the randomness of the channel. Thus as K_{ric} decreases, $\Gamma(d)$ would cross the connectivity threshold earlier with a higher probability (due to the increase in channel randomness), resulting in a smaller expected distance traveled.

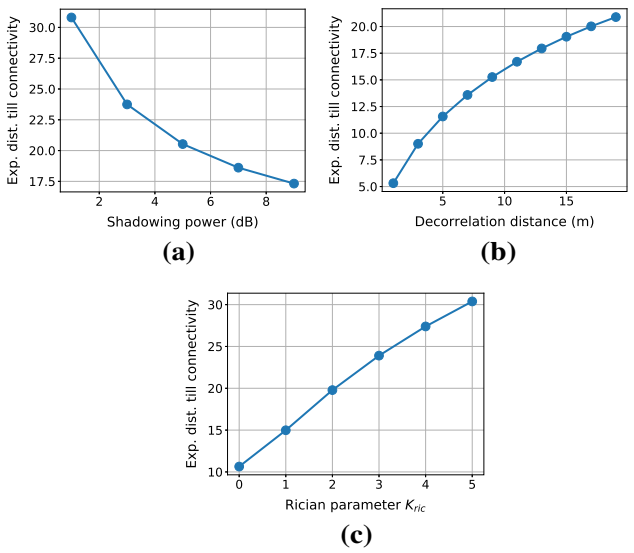

Fig. 9 Expected distance until connectivity (with multipath) as a function of the **a** shadowing power, **b** shadowing decorrelation distance and **c** Rician parameter K_{ric}, for the case of a straight path with $d_{\text{src}} = 550$ m and $\theta_{\text{src}} = 0$ rad

6 Conclusions

In this paper, we considered the scenario of a robot that seeks to get connected to another robot or a remote operator, as it moves along a path. We started by mathematically characterizing the PDF of the distance traveled until connectivity along straight paths, using a stochastic differential equation analysis when multipath can be ignored, and a recursive characterization for the case of multipath. We then developed a theoretical characterization of a more general space of loop-free paths, based on properties of the path such as its curvature, for which we can theoretically characterize the PDF of the FPD. Our characterizations not only enable new theoretical analysis but also allow for an efficient low-complexity implementation. Finally, we confirmed our theoretical results with simulations using two sets of real channel parameters from downtown San Francisco, and highlighted interesting trends of the FPD.

A Appendix

A.1 Proof of Lemma 2

Proof Let $r(s) = (x(s), y(s))$ be the equation of the path parameterized by arc length. Since the path is parameterized by arc length, we have

$$\|r'(s)\|^2 = |x'(s)|^2 + |y'(s)|^2 = 1. \tag{17}$$

Moreover, we have the curvature constraint

$$\|r''(s)\|^2 = |x''(s)|^2 + |y''(s)|^2 \leq \kappa^2. \tag{18}$$

Let s_0 denote the current point, i.e., the center of the ball. Without loss of generality, let $(x(s_0), y(s_0)) = (0, 0)$ and let the tangent at s_0 be parallel to the x-axis, i.e., $x'(s_0) = -1$, $y'(s_0) = 0$, as shown in Fig. 3c.

We first prove that no point of r_{ball} can lie outside the shaded region of Fig. 3c. Note that the shaded region has a boundary on the left corresponding to $x = -d_{\text{th}}$, and the two other boundaries correspond to circular arcs with curvature κ. Let us consider traveling backward along the path. For a given distance d_x traveled along the negative x-axis (i.e., $x(s) = -d_x$), the path which maximizes the distance traveled along the y-axis $|y(s)|$, is the one that minimizes the x-axis velocity $|x'(s)|$ and maximizes the y-axis velocity $|y'(s)|$ the most. This corresponds to the circular path $(R_c \cos(s/R_c), R_c \sin(s/R_c))$ with constant curvature κ. Thus, for any path satisfying (17) and (18), the y-axis coordinate is bounded above and below by the circular arc. This implies that the segment r_{ball} lies within the shaded region.

We next show that if $\kappa < 1/d_{\text{th}}$, then r_{ball} cannot loop within the ball. Note that, by definition, r_{ball} loops within the ball if $x'(s) > 0$ for some point on the path within the shaded region. The circular path with curvature κ is the path that maximizes $x'(s)$. From Fig. 3c, we can see that if $\kappa = 1/d_{\text{th}}$, then $x'(s) = 0$ at $x(s) = -d_{\text{th}}$ for the circular path. Thus, if $\kappa < 1/d_{\text{th}}$, we have $x'(s) > 0$ for any point of the path within the shaded region.

Finally, we determine the bound on the length of r_{ball}. If we travel a distance of d_{th} along the negative x-axis, then we are guaranteed to have exit the ball. The path that maximizes its length before covering d_{th} along the negative x-axis, would be the one that reduces the x-axis velocity $|x'(s)|$ the most. This maximal length path corresponds to the circular path with constant curvature κ. Any other path satisfying (17) and (18) would exit the shaded region before this circular path, i.e., the length of the segment of any path would be less that the length of this circular arc. The length of this circular arc can be found from the geometry of the figure. The chord length can be seen to be $2R_c \sin(\phi/2)$ where $R_c = 1/\kappa$. Moreover, we have $\cos(\phi/2) = \frac{d_{\text{th}}}{2R_c \sin(\phi/2)}$ which implies that $\phi = \sin^{-1}\left(\frac{d_{\text{th}}}{R_c}\right)$. This gives us the arc length as $2\pi R_c \times \frac{\phi}{2\pi} = R_c \sin^{-1}\left(\frac{d_{\text{th}}}{R_c}\right) = \frac{1}{\kappa}\sin^{-1}(\kappa d_{\text{th}})$. □

A.2 Proof of Lemma 5

Proof Using (8), we can show that $m = \alpha_1 \Gamma_{\text{SH},-1} + \alpha_r \Gamma_{\text{SH},r}$ where

$$\alpha_1 = \frac{e^{-d_1/\beta_{\text{SH}}} - e^{-(d_{1r}+d_r)/\beta_{\text{SH}}}}{1 - e^{-2d_{1r}/\beta_{\text{SH}}}},$$
$$\alpha_r = \frac{e^{-d_r/\beta_{\text{SH}}} - e^{-(d_1+d_{1r})/\beta_{\text{SH}}}}{1 - e^{-2d_{1r}/\beta_{\text{SH}}}}.$$

Then, the difference in mean $\Delta m = m - \hat{m}$ is distributed as $\mathcal{N}(0, \sigma^2_{\Delta m})$, where using (10) we have

$$\sigma^2_{\Delta m} = \sigma^2_{\text{SH}} \frac{\left(e^{-d_r/\beta_{\text{SH}}} - e^{-(d_1+d_{1r})/\beta_{\text{SH}}}\right)^2}{1 - e^{-2d_{1r}/\beta_{\text{SH}}}}.$$

Moreover, using (9) we can calculate

$$\frac{\sigma^2}{\sigma^2_{\text{SH}}} = 1 - \frac{e^{-2d_1/\beta_{\text{SH}}} + e^{-2d_r/\beta_{\text{SH}}} - 2e^{-(d_1+d_r+d_{1r})/\beta_{\text{SH}}}}{1 - e^{-2d_{1r}/\beta_{\text{SH}}}}.$$

The difference in variance $\Delta\sigma^2 = \sigma^2 - \hat{\sigma}^2$ can be calculated as

$$\Delta\sigma^2 = -\sigma^2_{\text{SH}} \frac{\left(e^{-d_r/\beta_{\text{SH}}} - e^{-(d_1+d_{1r})/\beta_{\text{SH}}}\right)^2}{1 - e^{-2d_{1r}/\beta_{\text{SH}}}} = -\sigma^2_{\Delta m}.$$

From (11), we then have

$$KL = \frac{\sigma^2_{\Delta m}}{2\hat{\sigma}^2}\chi^2_1 + \frac{1}{2}\left(-\frac{|\Delta\sigma^2|}{\hat{\sigma}^2} - \log_e\left(1 - \frac{|\Delta\sigma^2|}{\hat{\sigma}^2}\right)\right).$$

Since $\mathbb{E}[\chi^2_1] = 1$ and $\text{Var}[\chi^2_1] = 2$, we can calculate the mean m_{KL} and the standard deviation σ_{KL} to be as stated in the lemma. □

A.3 Proof of Lemma 6

Proof Consider all possible locations of the general point (see Fig. 4a) at a fixed distance d_r. From the geometry of Fig. 4a, we can see that $d_{1r} = \sqrt{d_1^2 + d_r^2 - 2d_1 d_r \cos\theta}$. Varying θ, results in varying d_{1r} which can take values in $[d_r - d_1, d_r + d_1]$. From Lemma 5, we can see that the θ that has a maximum impact on the KL divergence is the one that would minimize m_{KL} and σ_{KL}. This would occur when we maximize $\sigma^2_{\Delta m} = \sigma^2_{\text{SH}} e^{-d_r/\beta_{\text{SH}}} \frac{(1-e^{-(z-z_l)})^2}{1-e^{-2z}}$ where $z = d_{1r}/\beta_{\text{SH}}$ and $z_l = (d_r - d_1)/\beta_{\text{SH}}$. We wish to maximize $h(z) = \frac{(1-e^{-(z-z_l)})^2}{1-e^{-2z}}$. Taking it's derivative gives us

$$\frac{\mathrm{d}}{\mathrm{d}z}h(z) = \frac{2(1 - e^{-(z-z_l)})}{(1 - e^{-2z})^2}(e^{-(z-z_l)} - e^{-2z}).$$

Then $\frac{\mathrm{d}}{\mathrm{d}z}h(z) > 0$ if $z > -z_l$, which is true as long as $d_r > d_1$.

Thus, maximizing $\sigma^2_{\Delta m}$ occurs at $\theta = \pi$ where d_{1r} takes its maximum value of $d_1 + d_r$. Setting $\theta = \pi$ gives us

$$\sigma^2_{\Delta m} = \sigma^2_{\text{SH}} \frac{\left(e^{-d_r/\beta_{\text{SH}}} - e^{-(2d_1+d_r)/\beta_{\text{SH}}}\right)^2}{1 - e^{-2(d_1+d_r)/\beta_{\text{SH}}}}.$$

From Lemma 5, we can see that satisfying the KL divergence parameters implies that $\frac{\sigma^2_{\Delta m}}{\hat{\sigma}^2} \leq 1 - e^{-2\epsilon_m}$, and $\frac{\sigma^2_{\Delta m}}{\hat{\sigma}^2} \leq \sqrt{2}\epsilon_\sigma$. Let $\epsilon_d = \min\left\{1 - e^{-2\epsilon_m}, \sqrt{2}\epsilon_\sigma\right\}$. Thus, we obtain the constraint

$$\frac{e^{-2d_r/\beta_{\text{SH}}}(1-\rho^2)^2}{(1 - \rho^2 e^{-2d_r/\beta_{\text{SH}}})(1-\rho^2)} \leq \epsilon_d,$$

which in turn gives us the constraint

$$d_r \geq \frac{\beta_{\text{SH}}}{2}\log_e\left(\rho^2 + \frac{1-\rho^2}{\epsilon_d}\right).$$

□

A.4 Proof of Lemma 7

Proof Consider the scenario of Fig. 4b where $d_1 = \Delta d$. We will choose the location of the general point ($\Gamma_{\text{SH},r}$), which lies within the shaded region, such that it maximizes

the impact (in terms of the KL divergence) on the approximation. From Lemma 5, we can see that the point that has a maximum impact on the KL divergence is the one that would maximize $\sigma^2_{\Delta m}$. From the proof of Lemma 6, we know that for a fixed d_r and varying θ, the maximum value of $\sigma^2_{\Delta m}$ occurs at the maximum value of d_{1r}. This occurs at the boundary of the shaded region, i.e., at a point on the circular arc. Since this holds for all $d_1 < d_r \leq d_{\text{th}}$, we know that the point that maximizes $\sigma^2_{\Delta m}$ lies on the circular path with constant curvature κ.

We thus consider the setting in Fig. 4c with a fixed curvature κ. From the geometry of the figure, we have the following relations: $d_1 = 2R_c \sin\left(\frac{\Delta\phi}{2}\right)$, $d_{1r} = 2R_c \sin\left(\frac{\phi}{2}\right)$ and $d_r = 2R_c \sin\left(\frac{\phi+\Delta\phi}{2}\right)$. Since $d_1 = \Delta d$, we have $\Delta\phi = 2\sin^{-1}(\kappa\Delta d/2)$. From Lemma 3, we have the constraint that $\kappa < 1/d_{\text{th}}$. This guarantees that the path will leave the ball. Moreover, from the geometry of the figure, we can see that this will occur at the angle ϕ such that $d_r = 2R_c \sin\left(\frac{\phi+\Delta\phi}{2}\right) = d_{\text{th}}$. This occurs at $\phi = h_{\text{cons}}(\kappa) = 2\sin^{-1}(\frac{\kappa d_{\text{th}}}{2}) - \Delta\phi$.

From Lemma 5, we can see that satisfying the KL divergence parameters implies that $\frac{\sigma^2_{\Delta m}}{\hat{\sigma}^2} \leq 1 - e^{-2\epsilon_m}$, and $\frac{\sigma^2_{\Delta m}}{\hat{\sigma}^2} \leq \sqrt{2}\epsilon_\sigma$. Let $\epsilon_d = \min\left\{1 - e^{-2\epsilon_m}, \sqrt{2}\epsilon_\sigma\right\}$. Thus, the point on the path that maximizes the KL divergence occurs at the angle

$$\arg \max_{0<\phi\leq h_{\text{cons}}(\kappa)} h_{\text{opt}}(\kappa, \phi),$$

where

$$h_{\text{opt}}(\kappa, \phi) = \frac{\sigma^2_{\Delta m}}{\hat{\sigma}^2} = \frac{\left(e^{-\frac{2}{\kappa\beta_{\text{SH}}}\sin\left(\frac{\phi+\Delta\phi}{2}\right)} - \rho e^{-\frac{2}{\kappa\beta_{\text{SH}}}\sin\left(\frac{\phi}{2}\right)}\right)^2}{\left(1 - e^{-\frac{4}{\kappa\beta_{\text{SH}}}\sin\left(\frac{\phi}{2}\right)}\right)\left(1-\rho^2\right)}.$$

We wish to find the maximum curvature κ, such that this maximum impact still satisfies the KL divergence parameters, i.e.,

$$\max_{0<\phi\leq h_{\text{cons}}(\kappa)} h_{\text{opt}}(\kappa, \phi) \leq \epsilon_d.$$

This results in the optimization problem stated in the lemma. □

References

Abbasi, A. A., Younis, M., & Akkaya, K. (2009). Movement-assisted connectivity restoration in wireless sensor and actor networks. *IEEE Transactions on Parallel and Distributed Systems*, *20*(9), 1366–1379.

Caccamo, S., Parasuraman, R., Freda, L., Gianni, M., & Ogren, P. (2017). Rcamp: Resilient communication-aware motion planner and autonomous repair of wireless connectivity in mobile robots. In *IEEE/RSJ international conference on intelligent robots and systems (IROS)* (pp. 2153–0866).

Chatzipanagiotis, N., & Zavlanos, M. M. (2016). Distributed scheduling of network connectivity using mobile access point robots. *IEEE Transactions on Robotics*, *32*(6), 1333–1346.

Cover, T. M., & Thomas, J. A. (2012). *Elements of information theory*. New York: Wiley.

Craig, P. (2008). A new reconstruction of multivariate normal orthant probabilities. *Journal of the Royal Statistical Society: Series B (Statistical Methodology)*, *70*(1), 227–243.

Di Nardo, E., Nobile, A., Pirozzi, E., & Ricciardi, L. (2001). A computational approach to first-passage-time problems for Gauss–Markov processes. *Advances in Applied Probability*, *33*(2), 453–482.

Doob, J. L. (1949). Heuristic approach to the Kolmogorov–Smirnov theorems. *The Annals of Mathematical Statistics*, *20*(3), 393–403.

Dudley, R. M. (2002). *Real analysis and probability* (Vol. 74). Cambridge: Cambridge University Press.

Eberly D (2008) Moving along a curve with specified speed (p. 2). Preprint, see http://www.geometrictools.com.

Gardiner, C. (2009). *Stochastic methods: A handbook for the natural and social sciences*. Berlin: Springer.

Hashemi, H. (1994). A study of temporal and spatial variations of the indoor radio propagation channel. In *IEEE international symposium on personal, indoor and mobile radio communications* (pp. 127–134). IEEE.

Kay, S. M. (1993). *Fundamentals of statistical signal processing, volume i: Estimation theory (v. 1)*. Englewood Cliffs: PTR Prentice-Hall.

Kline, M. (1998). *Calculus: An intuitive and physical approach*. Courier Corporation.

Lancaster, H. O., & Seneta, E. (2005). Chi-square distribution. *Encyclopedia of Biostatistics*. https://doi.org/10.1002/0470011815.b2a15018.

Leblanc, B., & Scaillet, O. (1998). Path dependent options on yields in the affine term structure model. *Finance and Stochastics*, *2*(4), 349–367.

Malmirchegini, M., & Mostofi, Y. (2012). On the spatial predictability of communication channels. *IEEE Transactions on Wireless Communications*, *11*(3), 964–978.

Mehr, C., & McFadden, J. (1965). Certain properties of Gaussian processes and their first-passage times. *Journal of the Royal Statistical Society Series B (Methodological)*, *27*, 505–522.

Muralidharan, A., & Mostofi, Y. (2017a). Energy optimal distributed beamforming using unmanned vehicles. *IEEE Transactions on Control of Network Systems*, *5*(4), 1529–1540.

Muralidharan, A., & Mostofi, Y. (2017b). First passage distance to connectivity for mobile robots. In *American control conference (ACC)* (pp. 1517–1523). IEEE.

Muralidharan, A., & Mostofi, Y. (2017c). Path planning for a connectivity seeking robot. In *Globecom workshops (GC Wkshps)* (pp. 1–6). IEEE.

Papoulis, A., & Pillai, S. U. (2002). *Probability, random variables, and stochastic processes*. New York: Tata McGraw-Hill Education.

Rappaport, T. S. (1996). *Wireless communications: Principles and practice* (Vol. 2). Upper Saddle River: Prentice Hall PTR.

Ricciardi, L. M., & Sacerdote, L. (1979). The ornstein–uhlenbeck process as a model for neuronal activity. *Biological Cybernetics*, *35*(1), 1–9.
Ricciardi, L. M., & Sato, S. (1988). First-passage-time density and moments of the ornstein–uhlenbeck process. *Journal of Applied Probability*, *25*, 43–57.
Robert, C. P. (1996). Intrinsic losses. *Theory and Decision*, *40*(2), 191–214.
Siegert, A. J. (1951). On the first passage time probability problem. *Physical Review*, *81*(4), 617.
Smith, W. M., & Cox, D. C. (2004). *Urban propagation modeling for wireless systems*. Technical report, DTIC Document.
Tokekar, P., Vander Hook, J., Mulla, D., & Isler, V. (2016). Sensor planning for a symbiotic UAV and UGV system for precision agriculture. *IEEE Transactions on Robotics*, *32*(6), 1498–1511.
Yan, Y., & Mostofi, Y. (2012). Robotic router formation in realistic communication environments. *IEEE Transactions on Robotics*, *28*(4), 810–827.
Yan, Y., & Mostofi, Y. (2014). To go or not to go on energy-aware and communication-aware robotic operation. *IEEE Transactions on Control of Network Systems*, *1*(3), 218–231.
Zavlanos, M. M., Egerstedt, M. B., & Pappas, G. J. (2011). Graph-theoretic connectivity control of mobile robot networks. *Proceedings of the IEEE*, *99*(9), 1525–1540.
Zeng, Y., & Zhang, R. (2017). Energy-efficient UAV communication with trajectory optimization. *IEEE Transactions on Wireless Communications*, *16*(6), 3747–3760.

Arjun Muralidharan received the Bachelors degree in Electronics and Communication Engineering from the Indian Institute of Technology, Guwahati, in 2012 and the MS degree in Electrical and Computer Science Engineering (ECE) from the University of California, Santa Barbara (UCSB) in 2014. He is currently working towards his Ph.D. degree in the Department of Electrical and Computer Engineering at the University of California Santa Barbara. His research interests include cooperative robotic networks, game theory, wireless communications and information theory.

Yasamin Mostofi received the B.S. degree in electrical engineering from Sharif University of Technology, and the M.S. and Ph.D. degrees from Stanford University. She is currently a professor in the Department of Electrical and Computer Engineering at the University of California Santa Barbara. Yasamin is the recipient of the 2016 Antonio Ruberti Prize from the IEEE Control Systems Society, the Presidential Early Career Award for Scientists and Engineers (PECASE), the National Science Foundation (NSF) CAREER award, and the IEEE 2012 Outstanding Engineer Award of Region 6 (more than 10 Western U.S. states), among other awards. She was a semi-plenary speaker at the 2018 IEEE Conference on Decision and Control (CDC) and a keynote speaker at the 2018 Mediterranean Conference on Control and Automation (MED). Her research is at the intersection of communications and robotics, on mobile sensor networks. Current research thrusts include X-ray vision for robots, communication-aware robotics, human-robot collaboration, RF sensing, occupancy estimation, and see-through imaging. Her research has appeared in several reputable news venues such as BBC, Huffington Post, Daily Mail, Engadget, TechCrunch, NSF Science360, ACM News, and IEEE Spectrum, among others. She has served on the IEEE Control Systems Society conference editorial board 2008–2013. She is currently an associate editor for the IEEE TRANSACTIONS ON CONTROL OF NETWORK SYSTEMS.